

Stochastic Gradient Methods with Preconditioned Updates

Abdurakhmon Sadiev^{1,2,3} Aleksandr Beznosikov^{2,3} Abdulla Jasem Almansoori³
Dmitry Kamzolov³ Rachael Tappenden⁴ Martin Takáč³

¹ Ivannikov Institute for System Programming, Moscow, Russia

² Moscow Institute of Physics and Technology, Moscow, Russia

³ Mohamed bin Zayed University of Artificial Intelligence, Abu Dhabi, UAE

⁴ University of Canterbury, Christchurch, New Zealand

Abstract

This work considers the non-convex finite sum minimization problem. There are several algorithms for such problems, but existing methods often work poorly when the problem is badly scaled and/or ill-conditioned, and a primary goal of this work is to introduce methods that alleviate this issue. Thus, here we include a preconditioner based on Hutchinson’s approach to approximating the diagonal of the Hessian, and couple it with several gradient-based methods to give new ‘scaled’ algorithms: **Scaled SARAH** and **Scaled L-SVRG**. Theoretical complexity guarantees under smoothness assumptions are presented. We prove linear convergence when both smoothness and the PL condition are assumed. Our adaptively scaled methods use approximate partial second-order curvature information and, therefore, can better mitigate the impact of badly scaled problems. This improved practical performance is demonstrated in the numerical experiments also presented in this work.

1 Introduction

This work considers the following, possibly nonconvex, finite-sum optimization problem:

$$\min_{w \in \mathbb{R}^d} \left\{ P(w) = \frac{1}{n} \sum_{i=1}^n f_i(w) \right\}, \quad (1)$$

where $w \in \mathbb{R}^d$ is the model/weight parameter and the loss functions $f_i : \mathbb{R}^d \rightarrow \mathbb{R} \forall i \in [n] := \{1 \dots n\}$ are smooth and twice differentiable. Throughout this work it is assumed that (1) has an optimal solution, with a corresponding optimal value, denoted by w^* , and $P^* = P(w^*)$, respectively. Problems of the form (1) cover a plethora of applications, including empirical risk minimization, deep learning, and supervised learning tasks such as regularized least squares or logistic regression [Shalev-Shwartz and Ben-David, 2014]. This minimization problem can be difficult to solve, particularly when the number of training samples n , or problem dimension d , is large, or if the problem is nonconvex.

Stochastic Gradient Descent (SGD) is one of the most widely known methods for problem (1), and its origins date back to the 1950s with the work [Robbins and Monro, 1951]. The explosion of interest in machine learning has led to an immediate need for reliable and efficient algorithms for solving (1). Motivated by, and aiming to improve upon, vanilla SGD, many novel methods have already been developed for convex and/or strongly convex instances of (1), including SAG/SAGA [Le Roux et al., 2012, Defazio et al., 2014], SDCA [Shalev-Shwartz and Zhang, 2013],

SVRG [Johnson and Zhang, 2013, Xiao and Zhang, 2014], S2GD [Konečný and Richtárik, 2017] and SARAH [Nguyen et al., 2017], to name just a few. In general, these methods are simple, have low per iteration computational costs, and are often able to find an ε -optimal solution to (1) quickly, when $\varepsilon > 0$ is not too small. However, they often have several hyper-parameters that can be difficult to tune, they can struggle when applied to ill-conditioned problems, and many iterations may be required to find a high accuracy solution.

Non-convex instances of the optimization problem (1) (for example, arising from deep neural networks (DNNS)) have been diverting the attention of researchers of late, and new algorithms are being developed to fill this gap [Ghadimi and Lan, 2013, Ghadimi et al., 2016, Lei et al., 2017, Li et al., 2021b]. Of particular relevance to this work is the PAGE algorithm presented in [Li et al., 2021a]. The algorithm is conceptually simple, involving only one loop, and a small number of parameters, and can be applied to non-convex problems (1). The main update involves either a minibatch SGD direction, or the previous gradient with a small adjustment (similar to that in SARAH [Nguyen et al., 2017]). The Loopless SVRG (L-SVRG) method [Hofmann et al., 2015, Qian et al., 2021], is also of particular interest here. It is a simpler ‘loopless’ variant of SVRG, which, unlike for PAGE, involves an unbiased estimator of the gradient, and it can be applied to non-convex instances of problem (1).

For problems that are poorly scaled and/or ill-conditioned, second order methods that incorporate curvature information, such as Newton or quasi-Newton methods [Dennis Jr. and Moré, 1977, Fletcher, 1987, Nocedal and Wright, 2006], can often outperform first order methods. Unfortunately, they can also be prohibitively expensive, in terms of both computational and storage costs. There are several works that have tried to reduce the potentially high cost of second order methods by using only approximate, or partial curvature information. Some of these stochastic second order, and quasi-Newton [Jahani et al., 2021a, 2020] methods have shown good practical performance for some machine learning problems, although, possibly due to the noise in the Hessian approximation, sometimes they perform similarly to first order variants.

An alternative approach to enhancing search directions is to use a *preconditioner*. There are several methods for problems of the form (1), which use what we call a ‘first order preconditioner’ — a preconditioner built using gradient information — including Adagrad [Duchi et al., 2011], RMSProp [Tieleman et al., 2012], and Adam [Kingma and Ba, 2015]. Adagrad [Duchi et al., 2011] incorporates a diagonal preconditioner that is built using accumulated gradient information from the previous iterates. The preconditioner allows every component of the current gradient to be scaled adaptively, but it has the disadvantage that the elements of the preconditioner tend to grow rapidly as iterations progress, leading to a quickly decaying learning rate. A method that maintains the ability to adaptively scale elements of the gradient, but overcomes the drawback of a rapidly decreasing learning rate, is RMSProp. It does this by including a momentum parameter, β_2 in the update for the diagonal preconditioner. In particular, at each iteration the updated diagonal preconditioner is taken to be a convex combination (using a momentum parameter β_2) of the (square) of the previous preconditioner and the Hadamard product of the current gradient with itself. So, gradient information from all the previous iterates is included in the preconditioner, but there is a preference for more recent information. Adam [Kingma and Ba, 2015] combines the positive features of Adagrad and RMSProp, but it also uses a first moment estimate of the gradient, providing a kind of additional momentum. Adam performs well in practice, and is among the most popular algorithms for DNN.

Recently, second order preconditioners that use approximate and/or partial curvature information have been developed and studied. The approach in AdaHessian [Yao et al., 2020] was to use a diagonal preconditioner that was motivated by Hutchinson’s approximation to the diagonal of the Hessian [Bekas et al., 2007], but that also stayed close to some of the approximations used in existing methods such as Adam [Kingma and Ba, 2015] and Adagrad [Duchi et al.,

2011]. Because of this, the approximation often differed markedly from the true diagonal of the Hessian, and therefore it did not always capture good enough curvature information to be helpful. The work OASIS [Jahani et al., 2021b], proposed a preconditioner that was closely based upon Hutchinson’s approach, and provided a more accurate estimation of the diagonal of the Hessian, and correspondingly led to improved numerical behaviour in practice. The preconditioner presented in [Jahani et al., 2021b] is adopted here.

1.1 Notation and Assumptions

Given a Positive Definite (PD) matrix $D \in \mathbb{R}^{d \times d}$, the weighted Euclidean norm is defined to be $\|x\|_D^2 = x^T D x$, where $x \in \mathbb{R}^d$. The symbol \odot denotes the Hadamard product, and $\text{diag}(x)$ denotes the $d \times d$ diagonal matrix whose diagonal entries are the components of the vector $x \in \mathbb{R}^d$.

Recall that problem (1) is assumed to have an optimal (probably not a unique) solution w^* , with corresponding optimal value $P^* = P(w^*)$. As is standard for stochastic algorithms, the convergence guarantees presented in this work will develop a bound on the number of iterations T , required to push the expected squared norm of the gradient below some error tolerance $\varepsilon > 0$, i.e., to find a \hat{w}_T satisfying

$$\mathbb{E}[\|\nabla P(\hat{w}_T)\|_2^2] \leq \varepsilon^2. \quad (2)$$

A point \hat{w}_T satisfying (2) is referred to as an ε -optimal solution. Importantly, \hat{w}_T is *some* iterate generated in the first T iterations of each algorithm, but it is *not necessarily* the T th iterate. Throughout this work we assume that each $f_i : \mathbb{R}^d \rightarrow \mathbb{R}$ and $P : \mathbb{R}^d \rightarrow \mathbb{R}$ are twice differentiable and also L -smooth. This is formalized in the following assumption.

Assumption 1 (L -smoothness). For all $i \in [n]$ f_i and P are assumed to be twice differentiable and L -smooth, i.e., $\forall i \in [n], \forall w, w' \in \text{dom}(f_i)$ we have $\|\nabla f_i(w) - \nabla f_i(w')\| \leq L\|w - w'\|$, and $\forall w, w' \in \text{dom}(P)$ we have $\|\nabla P(w) - \nabla P(w')\| \leq L\|w - w'\|$.

For some of the results in this work, it will also be assumed that the function P satisfies the PL-condition. Note that the PL-condition does not imply convexity (see Footnote 1 in [Li et al., 2021a]).

Assumption 2 (Polyak-Łojasiewicz-condition). A function $P : \mathbb{R}^d \rightarrow \mathbb{R}$ satisfies the PL-condition if there exists $\mu > 0$, such that $\|\nabla P(w)\|^2 \geq 2\mu(P(w) - P^*)$, $\forall w \in \mathbb{R}^d$.

Note that in the case of the PL assumption, we can use the following definition of ε -optimal solution instead of (2):

$$\mathbb{E}[P(\hat{w}_T) - P^*] \leq \varepsilon. \quad (3)$$

1.2 Contributions

The main contributions of this work are stated below, and are summarized in Tables 1 and 2.

- **Scaled SARAH.** We present a new algorithm called **Scaled SARAH**, which is a combination of the SARAH [Nguyen et al., 2017] and PAGE [Li et al., 2021a] algorithms, coupled with the diagonal preconditioner from [Jahani et al., 2021b]. The inclusion of the preconditioner results in adaptive scaling of every element of the search direction (negative gradient), which leads to

Table 1: Comparison of scaled methods for non-convex problems. *Notation:* ε denotes solution accuracy (2). The ‘Tuning of β_2 ’ column shows whether it is easy (+), or difficult (−) to tune β_2 . Our preconditioner (6) works with any β_2 . Adam only supports certain large $\beta \approx 1$ [Défossez et al., 2020, Reddi et al., 2019].

Method	Reference	Convergence	Tuning of β_2
Adagrad	[Duchi et al., 2011]	ε^{-4}	+
	[Zou et al., 2018]		
	[Défossez et al., 2020]		
RMSProp	[Tieleman et al., 2012]	no theory	
Adam	[Kingma and Ba, 2015]	ε^{-4}	−
	[Défossez et al., 2020]		
AdaHessian	[Yao et al., 2020]	no theory	
OASIS	[Jahani et al., 2021b]	ε^{-4}	+
Scaled SARAH	This work	ε^{-2}	+
Scaled L-SVRG	This work	ε^{-2}	+

Table 2: A summary of the main results of this work. Complexities for Scaled SARAH and Scaled L-SVRG are given for nonconvex problems (first row), and under the PL assumption (second row). *Notation:* L = smoothness constant, μ = PL constant, ε = solution accuracy (2), $\Delta_0 = P(w^0) - P^*$, n = data size, and Γ, α are upper and lower bounds of the Hessian approximation.

	Scaled SARAH	Scaled L-SVRG
NC	$\mathcal{O}\left(n + \frac{\Gamma}{\alpha} \frac{\sqrt{n} L \Delta_0}{\varepsilon^2}\right)$	$\mathcal{O}\left(n + \frac{\Gamma}{\alpha} \frac{n^{2/3} L \Delta_0}{\varepsilon^2}\right)$
PL	$\mathcal{O}\left(\max\left\{n, \frac{\Gamma}{\alpha} \sqrt{n} \frac{L}{\mu}\right\} \log \frac{\Delta_0}{\varepsilon}\right)$	$\mathcal{O}\left(\max\left\{n, \frac{\Gamma}{\alpha} n^{2/3} \frac{L}{\mu}\right\} \log \frac{\Delta_0}{\varepsilon}\right)$

improved practical performance, particularly on ill-conditioned and poorly scaled problems. The algorithm is simple (a single loop) and is easy to tune (Section 3).

- **Scaled L-SVRG.** The Scaled L-SVRG algorithm is also presented, which is similar to L-SVRG, but with the addition of the diagonal preconditioner [Jahani et al., 2021b]. Again, the preconditioner allows all elements of the gradient to be scaled adaptively, the algorithm uses a single loop structure, and for this algorithm an unbiased estimate of the gradient is used. The inclusion of adaptive local curvature information via the preconditioner leads to improvements in practical performance.

- **Convergence guarantees.** Theoretical guarantees show that both Scaled SARAH and Scaled L-SVRG converge and we present an explicit bound for the number of iterations required by each algorithm to obtain an iterate that is ε -optimal. Convergence is guaranteed for both Scaled SARAH and Scaled L-SVRG under a smoothness assumption on the functions f_i . If both smoothness and the PL-condition hold, then improved iteration complexity results for Scaled SARAH and Scaled L-SVRG are obtained, which show that expected function value gap converges to zero at a linear rate (see Theorems 2 and 4). Our scaled methods achieve the best known rates of all methods with preconditioning for non-convex deterministic and stochastic problems, and Scaled SARAH and Scaled L-SVRG are the first preconditioned methods that achieve a linear rate of convergence under the PL assumption (see a detailed comparison in Section 5).

- **Numerical experiments.** Extensive numerical experiments were performed (Sections 6 and A) under various parameter settings to investigate the practical behaviour of our new scaled algorithms. The inclusion of preconditioning in Scaled SARAH and Scaled L-SVRG led to improvements in performance compared with no preconditioning in several of the experiments,

and Scaled SARAH and Scaled L-SVRG were competitive with, and often outperformed, Adam.

Paper outline. This paper is organised as follows. In Section 2 we describe the diagonal preconditioner that will be used in this work. In Section 3, we describe a new Scaled SARAH algorithm and present theoretical convergence guarantees. In Section 5, we discuss our results for the Scaled SARAH method and compare it with other state-of-the-art methods. In Section 4, we introduce the Scaled L-SVRG algorithm, which adapts the L-SVRG algorithm to include a preconditioner. We present numerical experiments demonstrating the practical performance of our proposed methods in Section 6. Concluding remarks are given in Section 7. All proofs (Sections D and E), additional numerical experiments (Section A), and further details and discussion can be found in the appendix.

2 Diagonal Preconditioner

In this section we describe the diagonal preconditioner that is used in this work. The paper [Bekas et al., 2007] described Hutchinson’s approximation to the diagonal of the Hessian, and this provided motivation for the diagonal preconditioner proposed in [Jahani et al., 2021b], which is adopted here. In particular, given an initial approximation D_0 , (to be described soon), and Hessian approximation momentum parameter $\beta \in (0, 1)$ (equivalent to the second moment hyperparameter, β_2 in Adam [Kingma and Ba, 2015]), for all $t \geq 1$,

$$D_t = \beta D_{t-1} + (1 - \beta) \text{diag} (z_t \odot \nabla^2 P_{\mathcal{J}_t}(w_t) z_t), \quad (4)$$

where z_t is a random vector with Rademacher distribution¹, \mathcal{J}_t is an index set randomly sampled from $[n]$, and

$$\nabla^2 P_{\mathcal{J}_t}(w_t) = \frac{1}{|\mathcal{J}_t|} \sum_{j \in \mathcal{J}_t} \nabla^2 f_j(w_t). \quad (5)$$

Finally, for $\alpha > 0$ (where the parameter $\alpha > 0$ is equivalent to the parameter ε in Adam [Kingma and Ba, 2015] and AdaHessian [Yao et al., 2020]), the diagonal preconditioner is:

$$\left(\hat{D}_t \right)_{i,i} = \max\{\alpha, |D_t|_{i,i}\}. \quad (6)$$

The expression (6) ensures that the preconditioner \hat{D}_t is always PD, so it is well-defined and results in a descent direction. The absolute values are necessary because the objective function is potentially nonconvex, so the batch Hessian approximation could be indefinite. In fact, even if the Hessian is PD, D_t in (4) may still contain negative elements due to the sampling strategy used.

The preconditioner (6) is a good estimate of the diagonal of the (batch) Hessian because Hutchinson’s updating formula (4) is used (see also Figures 12, 13). Hence, it captures accurate curvature information, which is helpful for poorly scaled and ill-conditioned problems. Because the preconditioner is diagonal it is easy and inexpensive to apply its inverse, and the associated storage costs are low.

The preconditioner (4)+(6) depends on the parameter β : if $\beta = 1$ then the preconditioner is fixed for all iterations, whereas if $\beta = 0$ then the preconditioner is simply a kind of sketched batch Hessian. Taking $0 < \beta < 1$ gives a convex combination of the previous approximation and the current approximation, thereby ensuring that the entire history is included in the preconditioner,

¹i.e., the components of the z_t are ± 1 with equal probability.

but is damped by β , and the most recent information is also present. See Section F for a detailed discussion of the choice of β .

The main computational cost of the approximation in (4) is the (batch) Hessian-vector product $\nabla^2 P_{\mathcal{J}_t}(w_t)z_t$. Fortunately, this can be efficiently calculated using two rounds of back propagation. Moreover, the preconditioner is matrix-free, simply needing an oracle to return the Hessian vector product, but it does not need explicit access to the batch Hessian itself; see Appendix B in [Jahani et al., 2021b]. Therefore, the costs (both computational and storage) for this preconditioner are not burdensome.

As previously mentioned, the approximation (4) requires an initial estimate D_0 of the diagonal of the Hessian, and this is critical to the success of the preconditioner. In particular, one must take

$$D_0 = \frac{1}{m} \sum_{j=1}^m \text{diag} (z_j \odot \nabla^2 P_{\mathcal{J}_j}(w_0)z_j), \quad (7)$$

where \mathcal{J}_j denotes sampled batches and the vectors z_j are generated from a Radermacher distribution. This ensures that \hat{D}_t does indeed approximate the diagonal of the Hessian; see Section 3.3 in [Jahani et al., 2021b].

The following remark confirms that the diagonal preconditioner is both PD and bounded.

Lemma 1 (See Remark 4.10 in [Jahani et al., 2021b]). For any $t \geq 1$, we have $\alpha I \preceq \hat{D}_t \preceq \Gamma I$, where $0 < \alpha \leq \Gamma = \sqrt{d}L$.

Note that Remark 4.10 is proved incorrectly in [Jahani et al., 2021b]. We reprove it in Appendix B.

3 Scaled SARAH

Here we propose a new algorithm, **Scaled SARAH**, for finite sum optimization (1). Our algorithm is similar to the **SARAH** algorithm [Nguyen et al., 2017] and the **PAGE** algorithm [Li et al., 2021a], but a key difference is that **Scaled SARAH** includes the option of a preconditioner, \hat{D}_t for all $t \geq 0$, with a preconditioned approximate gradient step. **Scaled SARAH** is presented now as Algorithm 1.

Algorithm 1 Scaled SARAH

- 1: **Input:** initial point w_0 , learning rate η , preconditioner \hat{D}_0 , probability p
 - 2: $v_0 = \nabla P(w_0)$
 - 3: **for** $t = 0, 1, 2, \dots$ **do**
 - 4: $w_{t+1} = w_t - \eta \hat{D}_t^{-1} v_t$
 - 5: Generate independently batches i_{t+1} for v_{t+1} and \mathcal{J}_t for \hat{D}_{t+1}
 - 6: $v_{t+1} = \begin{cases} \nabla P(w_{t+1}), & \text{with probability } p \\ v_t + \nabla f_{i_{t+1}}(w_{t+1}) - \nabla f_{i_{t+1}}(w_t), & \text{with probability } 1 - p \end{cases}$
 - 7: Update the preconditioner \hat{D}_{t+1}
 - 8: **end for**
 - 9: **Output:** \hat{w}_T chosen uniformly from $\{w_t\}_{t=0}^T$
-

In each iteration of Algorithm 1 an update is computed in Step 4. The point w_t is adjusted by taking a step in the direction $\hat{D}_t^{-1}v_t$, of fixed step size η . The vector v_t approximates the gradient, and the preconditioner scales that direction. A key difference between **Scaled SARAH** and **PAGE/SARAH** is the inclusion of the preconditioner \hat{D}_t^{-1} in this step.

Step 6 defines the next gradient estimator v_{t+1} , for which there are two options. With probability p the full gradient is used. Alternately, with probability $1 - p$, the new gradient estimate is the previous gradient approximation v_t , with an adjustment term that involves the difference between the gradient of f_i evaluated at w_{t+1} and at w_t . The search direction computed in **Scaled SARAH** contains gradient information, while the preconditioner described in Section 2 contains approximate second order information. When this preconditioner is applied to the gradient estimate, each dimension is scaled adaptively depending on the corresponding curvature. Intuitively, this amplifies dimensions with low curvature (shallow loss surfaces), while damping directions with high curvature (sharper loss surfaces). The aim is for $\hat{D}_t^{-1}v_t$ to point in a better, adjusted direction, compared with v_t .

Scaled SARAH is a single loop algorithm so it is conceptually simple. If $p = 1$ then the algorithm always picks the first option in Step 6, so that **Scaled SARAH** reduces to a preconditioned GD method. On the other hand, if $p = 0$, then only the second option in Step 6 is used.

Notice that **Scaled SARAH** is a combination of both the **PAGE** and **SARAH** algorithms, coupled with a preconditioner. **SARAH** [Nguyen et al., 2017] is a double loop algorithm, where the inner loop is defined in the same way as update in Step 6. **PAGE** [Li et al., 2021a] is based upon **SARAH**, but **PAGE** uses a single loop structure, and allows for minibatches to be used in the gradient approximation v_{t+1} (rather than the single component as in Step 6).² **Scaled SARAH** shares the same single loop structure as **PAGE**, but also shares the same single component update for the gradient estimator as **SARAH** (no minibatches). However, different from both **PAGE** and **SARAH**, **Scaled SARAH** uses a preconditioner in Step 4.

In the remainder of this work we focus on a particular instance of **Scaled SARAH**, which uses a fixed probability $p_t = p$, and uses the diagonal preconditioner presented in Section 2. These choices have been made because a central goal of this work is to understand the impact that a well chosen preconditioner has on poorly scaled problems. Convergence guarantees and the results of numerical experiments, will be presented using this set up.

Theoretical results for **Scaled SARAH** are presented now. In particular, we present complexity bounds on the number of iterations required by **Scaled SARAH** to obtain an ε -optimal solution for the non-convex problem (1) (recall Section 1.1 with (2) and (3)). The first result holds under Assumption 1, while the second theorem holds under both smoothness *and* PL assumptions. First, we define the following step-size bound:

$$\bar{\eta} = \frac{\alpha}{L \left(1 + \sqrt{\frac{1-p}{p}}\right)}. \quad (8)$$

Theorem 1. Suppose that Assumption 1 holds, let $\varepsilon > 0$, let p denote the probability, and let the step-size satisfy $\eta \leq \bar{\eta}$ (8). Then, the number of iterations performed by **Scaled SARAH**, starting from an initial point $w_0 \in \mathbb{R}^d$ with $\Delta_0 = P(w_0) - P^*$, required to obtain an ε -approximate solution of the non-convex finite-sum problem (1) can be bounded by

$$T = \mathcal{O} \left(\frac{\Gamma \Delta_0 L}{\alpha \varepsilon^2} \left(1 + \sqrt{\frac{1-p}{p}} \right) \right).$$

Theorem 2. Suppose that Assumptions 1 and 2 hold, let $\varepsilon > 0$, and let the step-size satisfy $\eta \leq \bar{\eta}$ (8). Then the number of iterations performed by **Scaled SARAH** sufficient for finding an

²Note that, while **PAGE** allows minibatches for either option in the update Step 6, most of the theoretical results presented in [Li et al., 2021a] require the full gradient to be computed as the first option in Step 6.

ε -approximate solution of non-convex finite-sum problem (1) can be bounded by

$$T = \mathcal{O} \left(\max \left\{ \frac{1}{p}, \frac{L \Gamma}{\mu \alpha} \left(1 + \sqrt{\frac{1-p}{p}} \right) \right\} \log \frac{\Delta_0}{\varepsilon} \right).$$

Note that this last theorem shows that **Scaled SARAH** exhibits a linear rate of convergence under both the smoothness assumption and the PL-condition.

We know that Algorithm 1 calls the full gradient at the beginning (Step 2) and then (in expectation) uses $pn + (1 - p)$ stochastic gradients for each iteration (Step 6). Thus, the number of stochastic gradient computations (i.e., gradient complexity) is $n + T[pn + (1 - p)]$ and the following corollaries of Theorems 1 and 2 are valid.

Corollary 1. Suppose that Assumption 1 holds, let $\varepsilon > 0$, let $p = \frac{1}{n+1}$, and let the step-size satisfy $\eta \leq \bar{\eta}$ (8). Then, the stochastic gradient complexity performed by **Scaled SARAH**, starting from an initial point $w_0 \in \mathbb{R}^d$ with $\Delta_0 = P(w_0) - P^*$, required to obtain an ε -approximate solution of the non-convex finite-sum problem (1) can be bounded by $\mathcal{O} \left(n + \frac{\Gamma \Delta_0 L}{\alpha \varepsilon^2} \sqrt{n} \right)$.

Corollary 2. Suppose that Assumptions 1 and 2 hold, let $\varepsilon > 0$, and let the step-size satisfy $\eta \leq \bar{\eta}$ (8). Then the stochastic gradient complexity performed by **Scaled SARAH** sufficient for finding an ε -approximate solution of non-convex finite-sum problem (1) can be bounded by $\mathcal{O} \left(\left\{ n + \frac{L \Gamma}{\mu \alpha} \sqrt{n} \right\} \log \frac{\Delta_0}{\varepsilon} \right)$.

4 Scaled L-SVRG

SVRG [Johnson and Zhang, 2013, Xiao and Zhang, 2014] is a variance reduced stochastic gradient method that is very popular for finite sum optimization problems. However, the algorithm has a double loop structure, and careful tuning of hyper-parameters is required for good practical performance.

Recently, in [Hofmann et al., 2015], it was proposed a Loopless **SVRG** (**L-SVRG**) variant, that has a simpler, single loop structure, which can be applied to problem (1) in the convex and smooth case. This was extended in [Qian et al., 2021] to cover the composite case with an arbitrary sampling scheme. With its single loop structure, and consequently fewer hyperparameters to tune, coupled with the fact that, unlike for **PAGE** (recall Section 1), **L-SVRG** uses an *unbiased* estimate of the gradient, **L-SVRG** is a versatile and competitive algorithm for problems of the form (1).

However, as for the other previously mentioned gradient based methods, **L-SVRG** can perform poorly when the problem is badly scaled and/or ill-conditioned. This provides the motivation for the **Scaled L-SVRG** method that we propose in this work. Our **Scaled L-SVRG** algorithm combines the positive features of **L-SVRG**, with a preconditioner, to give a method that is loopless, has few hyperparameters to tune, uses an unbiased estimate of the gradient, and adaptively scales the search direction depending upon the local curvature. The **Scaled L-SVRG** method is presented now as Algorithm 2.

Scaled L-SVRG can be described, in words, as follows. The algorithm is initialized with an initial main point w_0 and an initial reference point z_0 , a learning rate η , an initial direction $v_0 = \nabla P(w_0)$, an initial preconditioner \hat{D}_0 , and probability p . At each iteration $t \geq 0$ of **Scaled L-SVRG** (Algorithm 2) the new point w_{t+1} is taken to be a step from w_t in the *scaled* direction $\hat{D}_t^{-1} v_t$, of size η . The new point z_{t+1} is either the (unchanged) previous point z_t with probability p , or the scaled approximate gradient step w_{t+1} with probability $1 - p$. Next, we generate the

Algorithm 2 Scaled L-SVRG

- 1: **Input:** initial point w_0 , learning rate η , preconditioner \hat{D}_0 , probability p
 - 2: $z_0 = w_0, v_0 = \nabla P(w_0)$
 - 3: **for** $t = 0, 1, 2, \dots$ **do**
 - 4: $w_{t+1} = w_t - \eta \hat{D}_t^{-1} v_t$
 - 5: $z_{t+1} = \begin{cases} z_t, & \text{with probability } p \\ w_t, & \text{with probability } 1 - p \end{cases}$
 - 6: Generate independently batches i_{t+1} for v_{t+1} and \mathcal{J}_t for \hat{D}_{t+1}
 - 7: $v_{t+1} = \nabla f_{i_{t+1}}(w_{t+1}) - \nabla f_{i_{t+1}}(z_{t+1}) + \nabla P(z_{t+1})$
 - 8: Update the preconditioner \hat{D}_{t+1}
 - 9: **end for**
 - 10: **Output:** \hat{w}_T chosen uniformly from $\{w_t\}_{t=0}^T$
-

new search direction v_t . This is made up of the full gradient plus a small adjustment. Finally, the preconditioner is updated and the next iterate begins. The output, denoted by \hat{w}_T is chosen uniformly from the points w_t , for $t = 0, \dots, T$, generated by Scaled L-SVRG (Algorithm 2).

Note that a key difference between L-SVRG [Hofmann et al., 2015, Qian et al., 2021] and our new Scaled L-SVRG is the inclusion of the preconditioner in Step 4; recall that a competitive preconditioner is described in Section 2.

The following theorem presents a complexity bound on the number of iterations required by Scaled L-SVRG to obtain an ε -optimal solution for the non-convex problem (1).

Theorem 3. Suppose that Assumption 1 holds, let $\varepsilon > 0$, let p denote the probability and let the step-size satisfy $\eta \leq \min \left\{ \frac{\alpha}{4L}, \frac{\sqrt{p}\alpha}{\sqrt{24}L}, \frac{p^{2/3}}{144^{2/3}} \frac{\alpha}{L} \right\}$. Given an initial point $w_0 \in \mathbb{R}^d$, let $\Delta_0 = P(w_0) - P^*$. Then the number of iterations performed by Scaled L-SVRG, starting from w_0 , required to obtain an ε -approximate solution of non-convex finite-sum problem (1) can be bounded by

$$T = \mathcal{O} \left(\frac{\Gamma}{\alpha} \frac{L\Delta_0}{p^{2/3}\varepsilon^2} \right).$$

While the previous theorem held under a smoothness assumption, here we prove a complexity result for Scaled SARAH under both smoothness *and* PL assumptions.

Theorem 4. Suppose that Assumptions 1 and 2 hold, let $\varepsilon > 0$, let p denote the probability and let the step-size satisfy $\eta \leq \min \left\{ \frac{p\Gamma}{6\mu}, \frac{1}{4} \frac{\alpha}{L}, \left(\frac{p}{6}\right)^{1/2} \frac{\alpha}{L}, \left(\frac{p}{6}\right)^{2/3} \frac{\alpha}{L} \right\}$. Then the number of iterations performed by Scaled L-SVRG sufficient for finding an ε -approximate solution of non-convex finite-sum problem (1) can be bounded by

$$T = \mathcal{O} \left(\max \left\{ \frac{1}{p}, \frac{\Gamma}{\alpha} \frac{L}{p^{2/3}\mu} \right\} \log \frac{\Delta_0}{\varepsilon} \right).$$

Below we provide corollaries on the complexities of stochastic gradient.

Corollary 3. Suppose that Assumption 1 holds, let $\varepsilon > 0$, let $p = \frac{1}{n+1}$ and let the step-size satisfy $\eta \leq \min \left\{ \frac{\alpha}{4L}, \frac{\sqrt{p}\alpha}{\sqrt{24}L}, \frac{p^{2/3}}{144^{2/3}} \frac{\alpha}{L} \right\}$. Given an initial point $w_0 \in \mathbb{R}^d$, let $\Delta_0 = P(w_0) - P^*$. Then the stochastic gradient complexity performed by Scaled L-SVRG, starting from w_0 , required to obtain an ε -approximate solution of non-convex finite-sum problem (1) can be

bounded by $\mathcal{O}\left(n + \frac{\Gamma}{\alpha} \frac{L\Delta_0}{\varepsilon^2} n^{2/3}\right)$.

Corollary 4. Suppose that Assumptions 1 and 2 hold, let $\varepsilon > 0$, let $p = \frac{1}{n+1}$ and let the step-size satisfy $\eta \leq \min\left\{\frac{p\Gamma}{6\mu}, \frac{1}{4}\frac{\alpha}{L}, \left(\frac{p}{6}\right)^{1/2}\frac{\alpha}{L}, \left(\frac{p}{6}\right)^{2/3}\frac{\alpha}{L}\right\}$. Then the stochastic gradient complexity performed by Scaled L-SVRG sufficient for finding an ε -approximate solution of non-convex finite-sum problem (1) can be bounded by $\mathcal{O}\left(\left\{n + \frac{\Gamma}{\alpha} \frac{L}{\mu} n^{2/3}\right\} \log \frac{\Delta_0}{\varepsilon}\right)$.

5 Discussion

In this section, we discuss the theoretical results obtained for Scaled SARAH, Scaled L-SVRG and compare them with other scaled methods, as well as for methods without preconditioning. For convenience, we give Table 3 summarizing all the results.

- In Section 2 we consider scaling based on Hutchinson’s approximation, but our analysis can be used to obtain similar estimates for Scaled SARAH and Scaled L-SVRG with Adam preconditioning. In particular, we can prove an analog of Lemma 1 (see Appendix C) by additionally assuming boundedness of the stochastic gradient for all w : $\|\nabla f_i(w)\| \leq M$ (a similar assumption is made in [Défossez et al., 2020] for Adam). We present these results in Table 3 for comparison with the current best results for Adam.

- In the deterministic case, our results are significantly superior to those from [Défossez et al., 2020], in particular, in terms of the accuracy of the solution our estimates give $\mathcal{O}(\varepsilon^{-2})$ dependence, at the same time the guarantees from [Défossez et al., 2020] are $\mathcal{O}(\varepsilon^{-4})$. Compared to OASIS in the deterministic case, we have the same results in terms of ε , but our bounds are much better in terms of d , L , α . It is also an interesting detail that our estimates for Scaled SARAH and Scaled L-SVRG with Adam preconditioner are independent of d and with Hutchinson’s preconditioner depend on \sqrt{d} , which is important for high-dimensional problems.

- In the stochastic case, our convergence guarantees are also the best among other scaled methods, primarily in terms of ε . This is mainly due to the fact that we use the stochastic finite sum setting typical for machine learning.

- Unfortunately, our estimates are inferior to the bounds of the unscaled methods: SARAH and L-SVRG (the base methods for our methods) and SGD (the best-known method for minimization problems). As one can see in Table 3, all results for methods with preconditioning have the same problem. This is the level of theory development in this field at the moment. It seems that our results are able, in some sense, to reduce this gap between scaled and unscaled methods by decreasing the additional multiplier.

Summary. Our theoretical results exceed the estimates already in the literature for scaled methods. If we consider that algorithms with preconditioning are desirable from the point of view of real-world learning problems, it turns out that we prove the best results for the practical class of methods at present. Meanwhile, our estimates are still worse than those for unscaled methods. In Appendix F.1 we provide a possible explanation for why these estimates cannot be improved. In Section 6 we present experiments in which it becomes clear that real problems are not necessarily ”the worst”. On the contrary, practical problems are those where our method from Sections 2 and 3 shows its dominance.

Table 3: Comparison of deterministic and stochastic methods for non-convex problems in the general case and under Polyak-Łojasiewicz condition. In the stochastic case, the table is divided into two parts: the bounded and finite-sum setups. *Notation:* σ^2 = variance of stochastic gradients, M =uniform bound of (stochastic) gradients, the rest of the notation is the same as the one introduced earlier in the paper.

		Method and reference	Non-convex	Polyak-Łojasiewicz
Deterministic		SGD (Secs. B.2 and C.2 from [Li and Richtárik, 2020])	$\mathcal{O}\left(\frac{L\Delta_0}{\varepsilon^2}\right)$	$\mathcal{O}\left(\frac{L}{\mu} \log \frac{1}{\varepsilon}\right)$
		L-SVRG (Sec. 5 from [Qian et al., 2021])	$\mathcal{O}\left(\frac{L\Delta_0}{\varepsilon^2}\right)$	$\mathcal{O}\left(\frac{L}{\mu} \log \frac{1}{\varepsilon}\right)$
		SARAH (Sec. 3.2 from [Pham et al., 2020], Sec. 5 from [Li et al., 2021a])	$\mathcal{O}\left(\frac{L\Delta_0}{\varepsilon^2}\right)$	$\mathcal{O}\left(\frac{L}{\mu} \log \frac{1}{\varepsilon}\right)$
		Adagrad (Th. 1 from [Défossez et al., 2020])	$\tilde{\mathcal{O}}\left(\frac{dM^2}{\varepsilon^2} \cdot \frac{L\Delta_0}{\varepsilon^2}\right)$	—
		Adam (Sec. 4.3 from [Défossez et al., 2020])	$\tilde{\mathcal{O}}\left(\frac{dM^2}{\varepsilon^2} \cdot \frac{L\Delta_0}{\varepsilon^2}\right)$	—
		OASIS (Ths. 4.17 and 4.18 from [Jahani et al., 2021b])	$\mathcal{O}\left(\frac{dL^2}{\alpha^2} \cdot \frac{L\Delta_0}{\varepsilon^2}\right)$	$\mathcal{O}\left(\frac{dL^3}{\alpha^2\mu} \cdot \frac{L}{\mu} \log \frac{1}{\varepsilon}\right)$ ⁽¹⁾
		Scaled L-SVRG with Hutchinson’s preconditioner (ours)	$\mathcal{O}\left(\frac{\sqrt{dL}}{\alpha} \cdot \frac{L\Delta_0}{\varepsilon^2}\right)$	$\mathcal{O}\left(\frac{\sqrt{dL}}{\alpha} \cdot \frac{L}{\mu} \log \frac{1}{\varepsilon}\right)$
		Scaled L-SVRG with Adam preconditioner (ours)	$\mathcal{O}\left(\frac{M}{\alpha} \cdot \frac{L\Delta_0}{\varepsilon^2}\right)$	$\mathcal{O}\left(\frac{M}{\alpha} \cdot \frac{L}{\mu} \log \frac{1}{\varepsilon}\right)$
	Scaled SARAH with Hutchinson’s preconditioner (ours)	$\mathcal{O}\left(\frac{\sqrt{dL}}{\alpha} \cdot \frac{L\Delta_0}{\varepsilon^2}\right)$	$\mathcal{O}\left(\frac{\sqrt{dL}}{\alpha} \cdot \frac{L}{\mu} \log \frac{1}{\varepsilon}\right)$	
	Scaled SARAH with Adam preconditioner (ours)	$\mathcal{O}\left(\frac{M}{\alpha} \cdot \frac{L\Delta_0}{\varepsilon^2}\right)$	$\mathcal{O}\left(\frac{M}{\alpha} \cdot \frac{L}{\mu} \log \frac{1}{\varepsilon}\right)$	
Stochastic	Bounded variance	SGD (Secs. B.2 and C.2 from [Li and Richtárik, 2020])	$\mathcal{O}\left(\frac{L\Delta_0}{\varepsilon^2} + \frac{\sigma^2}{\varepsilon^2} \cdot \frac{L\Delta_0}{\varepsilon^2}\right)$	$\mathcal{O}\left(\frac{L}{\mu} \log \frac{1}{\varepsilon} + \frac{L\sigma^2}{\mu^2\varepsilon}\right)$
		Adagrad (Th. 1 from [Défossez et al., 2020])	$\tilde{\mathcal{O}}\left(\frac{dM^2}{\varepsilon^2} \cdot \frac{L\Delta_0}{\varepsilon^2} + d \cdot \frac{\sigma^2}{\varepsilon^2} \cdot \frac{L\Delta_0}{\varepsilon^2}\right)$	—
		Adam (Sec. 4.3 from [Défossez et al., 2020])	$\tilde{\mathcal{O}}\left(\frac{dM^2}{\varepsilon^2} \cdot \frac{L\Delta_0}{\varepsilon^2} + d \cdot \frac{\sigma^2}{\varepsilon^2} \cdot \frac{L\Delta_0}{\varepsilon^2}\right)$	—
		OASIS (Ths. 4.17 and 4.18 from [Jahani et al., 2021b])	$\mathcal{O}\left(\frac{dL^2}{\alpha^2} \cdot \frac{L\Delta_0}{\varepsilon^2} + \frac{dL^2}{\alpha^2} \cdot \frac{\sigma^2}{\varepsilon^2} \cdot \frac{L\Delta_0}{\varepsilon^2}\right)$	$\mathcal{O}\left(\frac{dL^3}{\alpha^2\mu} \cdot \frac{L}{\mu} \log \frac{1}{\varepsilon} + \frac{dL^2}{\alpha^2} \cdot \frac{L\sigma^2}{\mu^2\varepsilon}\right)$ ⁽¹⁾
	Finite-sum	L-SVRG (Sec. 5 from [Qian et al., 2021])	$\mathcal{O}\left(n + n^{2/3} \cdot \frac{L\Delta_0}{\varepsilon^2}\right)$	$\mathcal{O}\left(\left[n + n^{2/3} \cdot \frac{L}{\mu}\right] \log \frac{1}{\varepsilon}\right)$
		SARAH (Sec. 3.2 from [Pham et al., 2020], Sec. 5 from [Li et al., 2021a])	$\mathcal{O}\left(n + \sqrt{n} \cdot \frac{L\Delta_0}{\varepsilon^2}\right)$	$\mathcal{O}\left(\left[n + \sqrt{n} \cdot \frac{L}{\mu}\right] \log \frac{1}{\varepsilon}\right)$
		Scaled L-SVRG with Hutchinson’s preconditioner (ours)	$\mathcal{O}\left(\frac{\sqrt{dL}}{\alpha} \cdot n^{2/3} \cdot \frac{L\Delta_0}{\varepsilon^2}\right)$	$\mathcal{O}\left(\left[n + \frac{\sqrt{dL}}{\alpha} \cdot n^{2/3} \cdot \frac{L}{\mu}\right] \log \frac{1}{\varepsilon}\right)$
		Scaled L-SVRG with Adam preconditioner (ours)	$\mathcal{O}\left(\frac{M}{\alpha} \cdot n^{2/3} \cdot \frac{L\Delta_0}{\varepsilon^2}\right)$	$\mathcal{O}\left(\left[n + \frac{M}{\alpha} \cdot n^{2/3} \cdot \frac{L}{\mu}\right] \log \frac{1}{\varepsilon}\right)$
		Scaled SARAH with Hutchinson’s preconditioner (ours)	$\mathcal{O}\left(\frac{\sqrt{dL}}{\alpha} \cdot \sqrt{n} \cdot \frac{L\Delta_0}{\varepsilon^2}\right)$	$\mathcal{O}\left(\left[n + \frac{\sqrt{dL}}{\alpha} \cdot \sqrt{n} \cdot \frac{L}{\mu}\right] \log \frac{1}{\varepsilon}\right)$
		Scaled SARAH with Adam preconditioner (ours)	$\mathcal{O}\left(\frac{M}{\alpha} \cdot \sqrt{n} \cdot \frac{L\Delta_0}{\varepsilon^2}\right)$	$\mathcal{O}\left(\left[n + \frac{M}{\alpha} \cdot \sqrt{n} \cdot \frac{L}{\mu}\right] \log \frac{1}{\varepsilon}\right)$

⁽¹⁾ for strongly convex problems.

6 Numerical Experiments

The purpose of these numerical experiments is to study the practical performance of our new Scaled SARAH and Scaled L-SVRG algorithms, and hence, to understand the advantages of using the proposed diagonal preconditioner on SARAH and L-SVRG. These results will also be compared with SGD, both with and without the preconditioner described in Section 2, as well as the state-of-the-art (first order) preconditioned optimizer Adam.

We test these algorithms on problem (1) with two loss functions: (1) *logistic regression* loss function, which is convex, and (2) *non-linear least squares* loss function, which is nonconvex. The loss functions are described in details below. For further details and experimental results that support the findings of this section, please see Appendix A. Note that all the experiments were initialized at the point $w_0 = 0$, and each experiment was run for 10 different random seeds.

6.1 Loss Functions

Let $P(w)$ be the empirical risk on a dataset $\{(x_i, y_i)\}_{i=1}^n$ where $x_i \in \mathbb{R}^d$ and $y_i \in \{-1, +1\}$. Then, the *logistic regression loss* is

$$P_{\text{logistic}}(w) = \frac{1}{n} \sum_{i=1}^n \log(1 + e^{-y_i x_i^T w}) \quad (9)$$

whereas for $y_i \in \{0, 1\}$ the *non-linear least squares loss (NLLSQ)* is

$$P_{\text{nllsq}}(w) = \frac{1}{n} \sum_{i=1}^n (y_i - 1/(1 + e^{-x_i^T w}))^2 \quad (10)$$

We consider two different loss functions to test our algorithms on both convex and nonconvex settings.

6.2 Binary Classification on LibSVM Datasets

We train the optimizers on three binary classification LibSVM datasets³, namely `w8a`, `rcv1`, and `real-sim`. We also consider feature-scaled versions of these datasets, where the scaling is done as follows: we choose a minimum exponent k_{\min} and a maximum exponent k_{\max} , and scale the features by values ranging from $10^{k_{\min}}$ to $10^{k_{\max}}$ in equal steps in the exponent according to the number of features and in random order. The setting $(k_{\min}, k_{\max}) = (0, 0)$ corresponds to the original, unscaled version of the datasets. We consider combinations of $k_{\min} = 0, -3$ and $k_{\max} = 0, 3$. This scaling is done to check the robustness and overall effectiveness of the diagonal preconditioner in comparison with Adam.

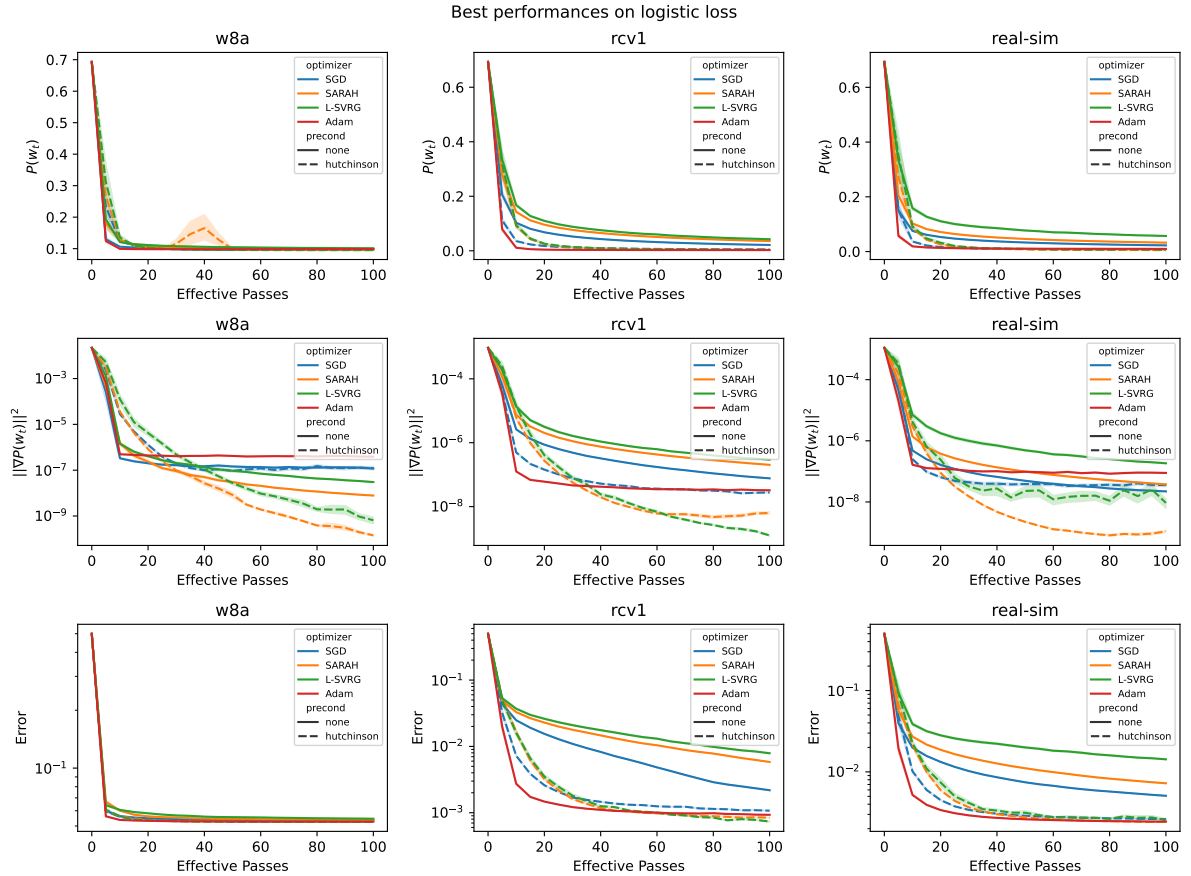


Figure 1: Best performances of the optimizers, including Adam, on the (unscaled) LibSVM datasets using the logistic loss. The Scaled variants are shown as dashed lines sharing the same color.

Figure 1 shows the results of the first experiment, and presents three types of line plots for each of the datasets of interest where the loss function is the logistic regression loss (9). Figure 2

³<https://www.csie.ntu.edu.tw/~cjlin/libsvmtools/datasets/>

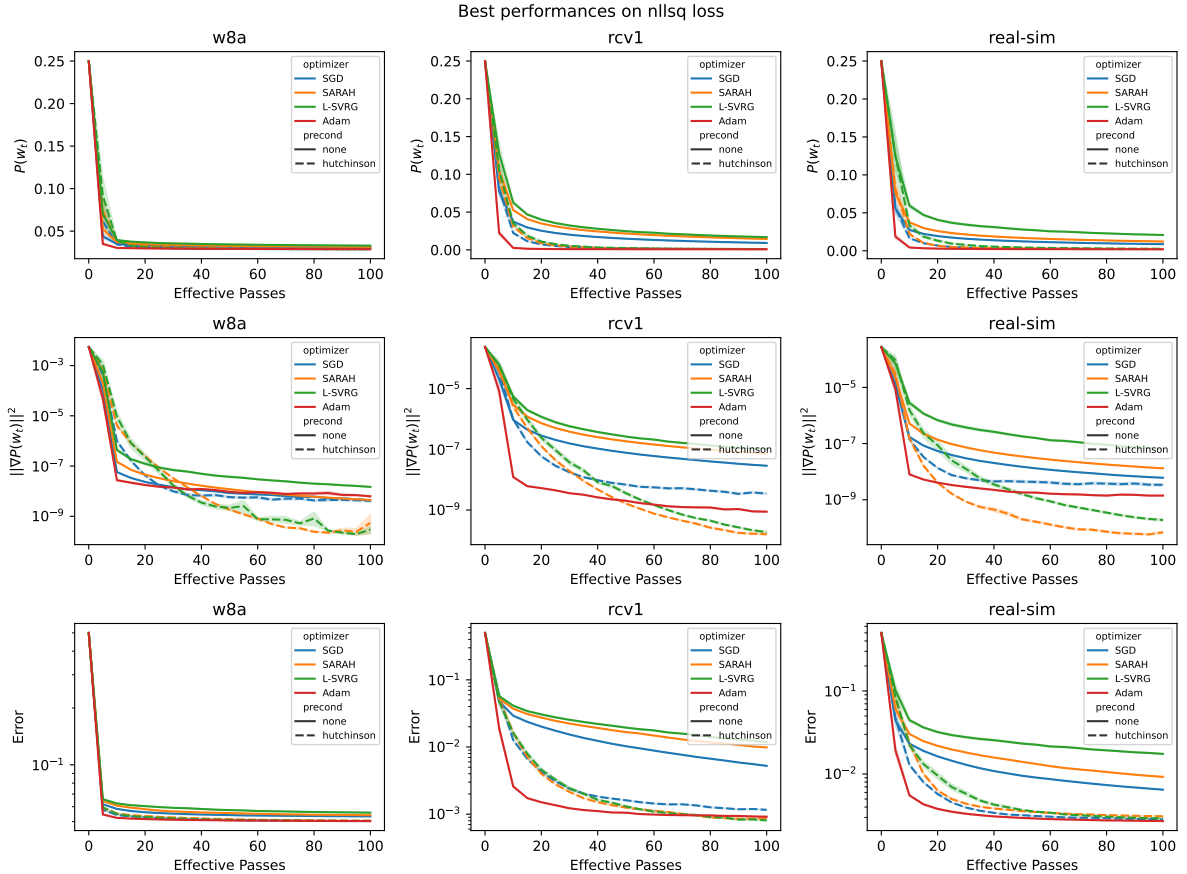


Figure 2: Best performances on the unscaled LibSVM datasets using the NLLSQ loss.

shows the same for the NLLSQ loss (10). The first row corresponds to the loss, the second is the squared norm of the gradient, and the third is the error. Tuning was performed in order to select the best hyperparameters (that minimize either the loss, gradient norm squared, or the error). The hyperparameter search grid is reported in Appendix, Table 4, and a thorough discussion is below. We fixed the batch size to be 128, in order to narrow the fine-tuned variables down to η , β , and α . Figure 1 shows the performances when minimizing the error on the unscaled datasets, $(k_{min}, k_{max}) = (0, 0)$. Experiments on scaled datasets can be found in Appendix A.2.

We can see from Figures 1 and 2 that the scaled versions of SGD, SARAH, and L-SVRG always improve on their non-scaled versions. In fact, they perform better than Adam in most cases. Initial convergence of Adam might be faster, but after enough effective passes, we can see that the scaled algorithms can generalize better. We also show similar performance improvement on deep neural nets in A.6.

In order to understand the main factors that affect the preconditioner, we ran comparative studies, including studying the parameters β , and α , as well as studying the initialization of preconditioner D_0 , including a warm-up period, and studying how the number of samples, z , impacts performance. First, recalling (7), there did not appear to be any significant improvement from averaging across more samples of z per minibatch, neither in the initialization nor in the update step. We also observed that initializing D_0 with a batch size of 100 was sufficiently good for non-sparse problems, and consistently resulted in a relative error of within 0.1 from the true diagonal. However, increasing the number of warm-up samples, proportionally to the number of features, led to observable improvements in convergence for sparse datasets.

We also investigated the role that β (4) played in algorithm performance. We found that

larger values lead to slightly slower but more stable convergence. The best β highly depends on the dataset, but the value 0.999 appeared to be a good starting point in general. To ensure a fair comparison, we also optimized Adam’s momentum parameter β_2 over the same range.

Aside from the batch size and learning rate, we found that, for ill-conditioned problems, the choice of α (recall (6) and Lemma 1) played an important role in determining the quality of the solution, convergence speed, and stability (which is not obvious from Figure 1). For example, if the features were scaled with $k_{min} = -3$ and $k_{max} = 0$, the best α is often around 10^{-7} (very small), whereas if we scaled with $k_{min} = 0$ and $k_{max} = 3$, the best α becomes 10^{-1} (relatively large). Therefore, finding the best α might require some additional fine-tuning, depending on the choice of η and β . However, we noticed that once we had tuned the learning rate for one scaled version of the dataset, the same learning rate transferred well to all the other scaled versions. In general, the optimal learning rate in our Scaled algorithms is very robust to feature scaling, given that α is chosen well, whereas Adam’s learning rate depends more heavily upon how ill-conditioned the problem is, so it requires fine-tuning across a potentially much wider range. In our case, tuning α and β is straightforward, so we obtained state-of-the-art performance with minimal parameter tuning.

The choice $\beta = 1 - 1/(t + 1)$ was investigated in Appendices A.5 and F.3. Preliminary results suggest that this choice virtually removes the dependence on α , and is competitive with a fine-tuned β across a large number of values. This makes fine-tuning much easier, even for strong feature scaling.

7 Conclusion

This paper investigates optimization methods with scaling for finite sum stochastic problems. The proposed algorithms are based on well-known variance reduction techniques: SARAH/PAGE, SVRG/L-SVRG. In addition to the basic updates, gradient preconditioning matrices are used to allow individually adapting steps for each optimization variable. Rather general assumptions on these matrices (diagonality and positive spectrum) give opportunity to analyze combinations of variance reduction approaches with popular scaling techniques: RMSProp, Adam, OASIS. Meanwhile, the unification of the assumptions gives the weakness of the result in some sense. The theoretical guarantees of convergence are no better than for the simple unscaled methods. Therefore, while the paper improves the results of methods with scaling for stochastic problems, it does not address the key question of why these methods can be better than the basic algorithms. This is an interesting and important direction for the future research.

Acknowledgements

The work of A. Sadiev was supported by a grant for research centers in the field of artificial intelligence, provided by the Analytical Center for the Government of the Russian Federation in accordance with the subsidy agreement (agreement identifier 000000D730321P5Q0002) and the agreement with the Ivannikov Institute for System Programming of the Russian Academy of Sciences dated November 2, 2021 No. 70-2021-00142.

References

- C. Bekas, E. Kokiopoulou, and Y. Saad. An estimator for the diagonal of a matrix. *Applied Numerical Mathematics*, 57(11):1214–1229, 2007. Numerical Algorithms, Parallelism and Applications (2).

- A. Defazio, F. Bach, and S. Lacoste-Julien. SAGA: A fast incremental gradient method with support for non-strongly convex composite objectives. In *Proceedings of the 27th International Conference on Neural Information and Processing Systems*, vol. 1, pages 1646–1654, 2014.
- A. Défossez, L. Bottou, F. Bach, and N. Usunier. A simple convergence proof of adam and adagrad. *arXiv preprint arXiv:2003.02395*, 2020.
- J. E. Dennis Jr. and J. J. Moré. Quasi-newton methods, motivation and theory. *SIAM Review*, 19(1):46–89, 1977.
- J. Duchi, E. Hazan, and Y. Singer. Adaptive subgradient methods for online learning and stochastic optimization. *Journal of Machine Learning Research*, 12(7):2121–2159, 2011.
- R. Fletcher. *Practical Methods of Optimization*. John Wiley & Sons, New York, 2 edition, 1987.
- S. Ghadimi and G. Lan. Stochastic first- and zeroth-order methods for nonconvex stochastic programming. *SIAM Journal on Optimization*, 23(4):2341–2368, 2013.
- S. Ghadimi, G. Lan, and H. Zhang. Mini-batch stochastic approximation methods for nonconvex stochastic composite optimization. *Mathematical Programming*, 155:267–305, 2016.
- T. Hofmann, A. Lucchi, S. Lacoste-Julien, and B. McWilliams. Variance reduced stochastic gradient descent with neighbors. In *Proceedings of the 28th International Conference on Neural Information and Processing Systems*, pages 2305–2313, 2015.
- M. Jahani, M. Nazari, S. Rusakov, A. Berahas, and M. Takáč. Scaling up quasi-Newton algorithms: Communication efficient distributed SR1. In *International Conference on Machine Learning, Optimization and Data Science*, pages 41–54, 2020. PMLR.
- M. Jahani, M. Nazari, R. Tappenden, A. Berahas, and M. Takáč. SONIA: a symmetric blockwise truncated optimization algorithm. In *International Conference on Artificial Intelligence and Statistics*, pages 487–495, 2021a. PMLR.
- M. Jahani, S. Rusakov, Z. Shi, P. Richtárik, M. Mahoney, and M. Takáč. Doubly adaptive scaled algorithm for machine learning using second-order information. *arXiv preprint arXiv:2109.05198v1*, 2021b.
- R. Johnson and T. Zhang. Accelerating stochastic gradient descent using predictive variance reduction. In *Proceedings of the 26th International Conference on Neural Information and Processing Systems*, vol. 1, pages 315–323, 2013.
- D. P. Kingma and J. Ba. Adam: A method for stochastic optimization. In *International Conference on Learning Representations*, pages 2305–2313, 2015.
- J. Konečný and P. Richtárik. Semi-stochastic gradient descent methods. *Frontiers in Applied Mathematics and Statistics*, 3, 2017.
- N. L. R. Le Roux, M. Schmidt, and F. Bach. A stochastic gradient method with an exponential convergence rate for finite training sets. In *Proceedings of the 25th International Conference on Neural Information and Processing Systems*, vol. 2, pages 2663–2671, 2012.
- Y. Lecun, L. Bottou, Y. Bengio, and P. Haffner. Gradient-based learning applied to document recognition. *Proceedings of the IEEE*, 86(11):2278–2324, 1998. doi: 10.1109/5.726791.

- L. Lei, C. Ju, J. Chen, and M. Jordan. Non-convex finite-sum optimization via SCSG methods. In *Proceedings of the 31st International Conference on Neural Information and Processing Systems*, pages 2345–2355, 2017.
- Z. Li and P. Richtárik. A unified analysis of stochastic gradient methods for nonconvex federated optimization. *arXiv preprint arXiv:2006.07013*, 2020.
- Z. Li, H. Bao, X. Zhang, and P. Richtarik. PAGE: A simple and optimal probabilistic gradient estimator for nonconvex optimization. In *Proceedings of the 38th International Conference on Machine Learning*, PMLR 139, pages 6286–6295, 2021a.
- Z. Li, S. Hanzely, and P. Richtárik. ZeroSARAH: Efficient nonconvex finite-sum optimization with zero full gradient computation. *arXiv preprint arXiv:2103.01447*, 2021b.
- L. M. Nguyen, J. Liu, K. Scheinberg, and M. Takáč. SARAH: A novel method for machine learning problems using stochastic recursive gradient. In *Proceedings of the 34th International Conference on Machine Learning*, PMLR 70, pages 2613–2621, 2017.
- J. Nocedal and S. J. Wright. *Numerical Optimization*. Springer Series in Operations Research, 2 edition, 2006.
- A. Paszke, S. Gross, F. Massa, A. Lerer, J. Bradbury, G. Chanan, T. Killeen, Z. Lin, N. Gimelshein, L. Antiga, A. Desmaison, A. Kopf, E. Yang, Z. DeVito, M. Raison, A. Tejani, S. Chilamkurthy, B. Steiner, L. Fang, J. Bai, and S. Chintala. Pytorch: An imperative style, high-performance deep learning library. In H. Wallach, H. Larochelle, A. Beygelzimer, F. d'Alché-Buc, E. Fox, and R. Garnett, editors, *Advances in Neural Information Processing Systems 32*, pages 8024–8035. Curran Associates, Inc., 2019. URL <http://papers.neurips.cc/paper/9015-pytorch-an-imperative-style-high-performance-deep-learning-library.pdf>.
- N. H. Pham, L. M. Nguyen, D. T. Phan, and Q. Tran-Dinh. Proxsarah: An efficient algorithmic framework for stochastic composite nonconvex optimization. *J. Mach. Learn. Res.*, 21(110): 1–48, 2020.
- X. Qian, Z. Qu, and P. Richtárik. L-SVRG and L-katyusha with arbitrary sampling. *Journal of Machine Learning Research*, 22:1–49, 2021.
- S. J. Reddi, S. Kale, and S. Kumar. On the convergence of adam and beyond. *arXiv preprint arXiv:1904.09237*, 2019.
- H. Robbins and S. Monro. A stochastic approximation method. *The Annals of Mathematical Statistics*, 22(3):400–407, 1951.
- S. Shalev-Shwartz and S. Ben-David. *Understanding machine learning: From theory to algorithms*. Cambridge university press, 2014.
- S. Shalev-Shwartz and T. Zhang. Stochastic dual coordinate ascent methods for regularized loss minimization. *Journal of Machine Learning Research*, 14(1):567–599, 2013.
- T. Tieleman, G. Hinton, et al. Lecture 6.5-rmsprop: Divide the gradient by a running average of its recent magnitude. *COURSERA: Neural networks for machine learning*, 4(2):26–31, 2012.
- L. Xiao and T. Zhang. A proximal stochastic gradient method with progressive variance reduction. *SIAM Journal on Optimization*, 24(4):2057–2075, 2014.

- Z. Yao, A. Gholami, S. Shen, K. Keutzer, and M. W. Mahoney. ADAHESSIAN: An adaptive second order optimizer for machine learning. *arXiv preprint arXiv:2006.00719*, 2020.
- F. Zou, L. Shen, Z. Jie, J. Sun, and W. Liu. Weighted adagrad with unified momentum. *arXiv preprint arXiv:1808.03408*, 2018.

A Additional numerical experiments

Here we provide additional details related to our experimental set-up, as well as presenting the results of additional numerical experiments.

A.1 Best performance given a fixed parameter

Table 4 states the hyperparameters that were used in our numerical experiments.

Table 4: Hyperparameter search grid.

Settings	
Optimizer	SARAH, L-SVRG, SGD, Adam
Scaled	True, False (except for Adam)
Dataset	a9a, w8a, rcv1, real-sim
(k_{min}, k_{max})	(0, 0), (0, 3), (-3, 0), (-3, 3)
Loss function	logistic, NLLSQ
Random Seed	0, \dots , 9
Parameters	
Batch Size	128, 512
η	$2^{-20}, 2^{-18}, \dots, 2^4$
α	$10^{-1}, 10^{-3}, 10^{-7}$
β	0.95, 0.99, 0.995, 0.999, avg

We ran extensive experiments in order to find the best performing set of parameters for each optimizer on each dataset. For our parameter search, we fixed one parameter (e.g., $\alpha = 10^{-1}$), and then found the best choice for the remaining parameters, given that fixed value. This allowed us to understand how robust the algorithm’s optimal performance is, with respect to each parameter. In other words, ‘how does changing one parameter degrade the quality of the solution or the overall performance of the algorithm?’. We also report the best overall performances.

Here, we consider fixing one of three parameters: η , β , and α , and then plot the trajectory of the gradient norm squared $\|\nabla P(w_t)\|^2$ for the setting that minimizes the error with respect to the other parameters. The values ‘ $\alpha = \text{none}$ ’ and ‘ $\beta = \text{none}$ ’ indicate non-preconditioned trajectories, and the value $\beta = \text{avg}$ indicate the choice $\beta_t = 1 - 1/(t + 1)$ (or more precisely, as described in Appendix A.5). See Figures 3, 4, 5, and 6.

A.2 Corrupting scale of features

We consider the settings where the features of the data are corrupted with a given logarithmic scale. We show the best overall performances on 4 scaled datasets with $(k_{min}, k_{max}) \in \{(-3, 0), (0, 3), (-3, 3)\}$. This allowed us to understand the impact of no preconditioning versus preconditioning on poorly scaled problems. The results are shown in Figures 7, 8, and 9.

A.3 Convex vs. non-convex loss

We test our algorithms on the non-linear least squares loss, which is a non-convex loss function. We show the best performance on the unscaled datasets, as well as datasets scaled with $(k_{min}, k_{max}) = (-3, 3)$. See Figures 10, and 11.

A.4 Relative error of D_0

For the preconditioner described in Section 2, the initial preconditioner D_0 must be chosen appropriately. Note that, if $\text{diag}(H_0)$ is the true Hessian diagonal for some initial point w_0 , then the relative error of the approximation D_0 to $\text{diag}(H_0)$ is

$$\frac{\|D_0 - \text{diag}(H_0)\|}{\|\text{diag}(H_0)\|}.$$

For our numerical experiments we used this relative error to determine whether the initial preconditioner D_0 was sufficiently accurate. In particular, we noticed that, if a minibatch of size 100 was used, then the resulting D_0 almost always reached a relative error of below 0.1, for dense datasets. For sparse datasets, more warm-up samples can improve convergence and quality of the solution, but in either case, a minibatch of size 100 was sufficient to establish convergence. Thus, we initialized D_0 with a size 100 minibatch in most of our experiments. See Figures 12, 13, and 14.

A.5 Choosing β_t

We show plots where we finetune α and β on a wider range of parameters. Similarly to Section A.1, we optimize the other parameters by fixing the parameter of interest at the chosen value, and report the optimal performance metric. We only consider **Scaled SARAH** in this experiment. We show plots where we minimize either the error or the gradient norm under the logistic loss or NLLSQ loss. We also show the optimal performance when choosing $\beta_t = 1 - \frac{1}{t+t_0}$, where t_0 is the number of warm-up samples. We run experiments for 10 random seeds and show the confidence intervals for each hyperparameter setting. We see that the suggested choice for β_t is consistently competitive with the best β and is robust to feature scaling as well. See Figures 15, 16, and 17.

A.6 Deep neural nets on MNIST

In order to demonstrate that our algorithms are indeed practical and competitive with the state-of-the-art, we test them on deep neural nets. The setting of our experiment is widely accessible and well-known; train the LeNet-5 model on MNIST dataset with the cross entropy loss [Lecun et al., 1998]. For this experiment, we believe that it suffices to test **Scaled L-SVRG** vs. **Adam**. For L-SVRG, we use $p = 0.999$. The programming framework we run this experiment on is PyTorch [Paszke et al., 2019]. The hyperparameter search grid is slightly reduced for this experiment. To be specific, learning rates bigger than 2^{-6} and lower than 2^{-14} are omitted, and we only consider β in $\{\text{avg}, 0.99, 0.999\}$. The result is shown in Figure 18, 19 and 20. We observe that the performance of **Scaled L-SVRG** is indeed competitive with **Adam** in this simple deep learning problem. We omit trajectories that diverge in this plot, which is why the value $\alpha = 10^{-7}$ is not seen in Figure 20. In the future, we plan on running more sophisticated deep learning experiments, and explore ways to adapt our algorithms to these settings in particular.

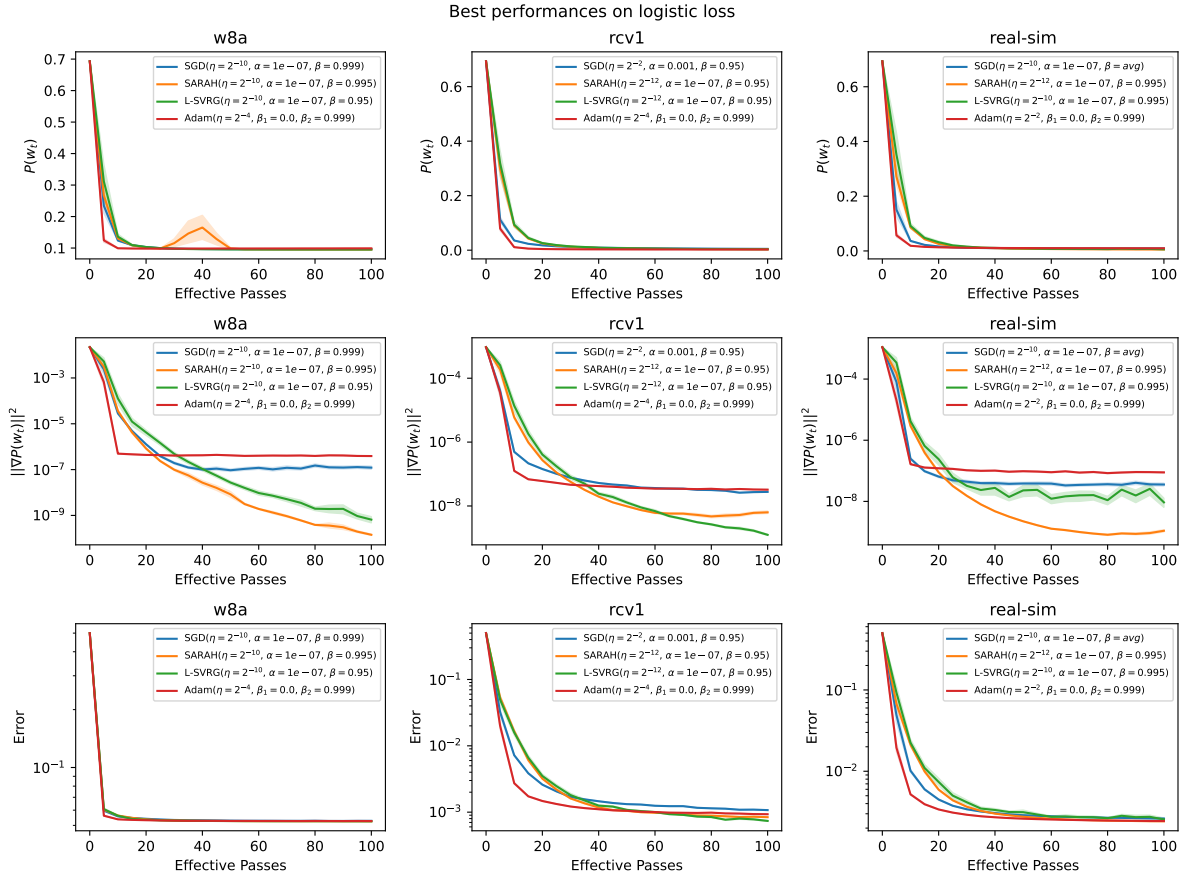


Figure 3: Performance of the best parameters minimizing the error using the logistic loss.

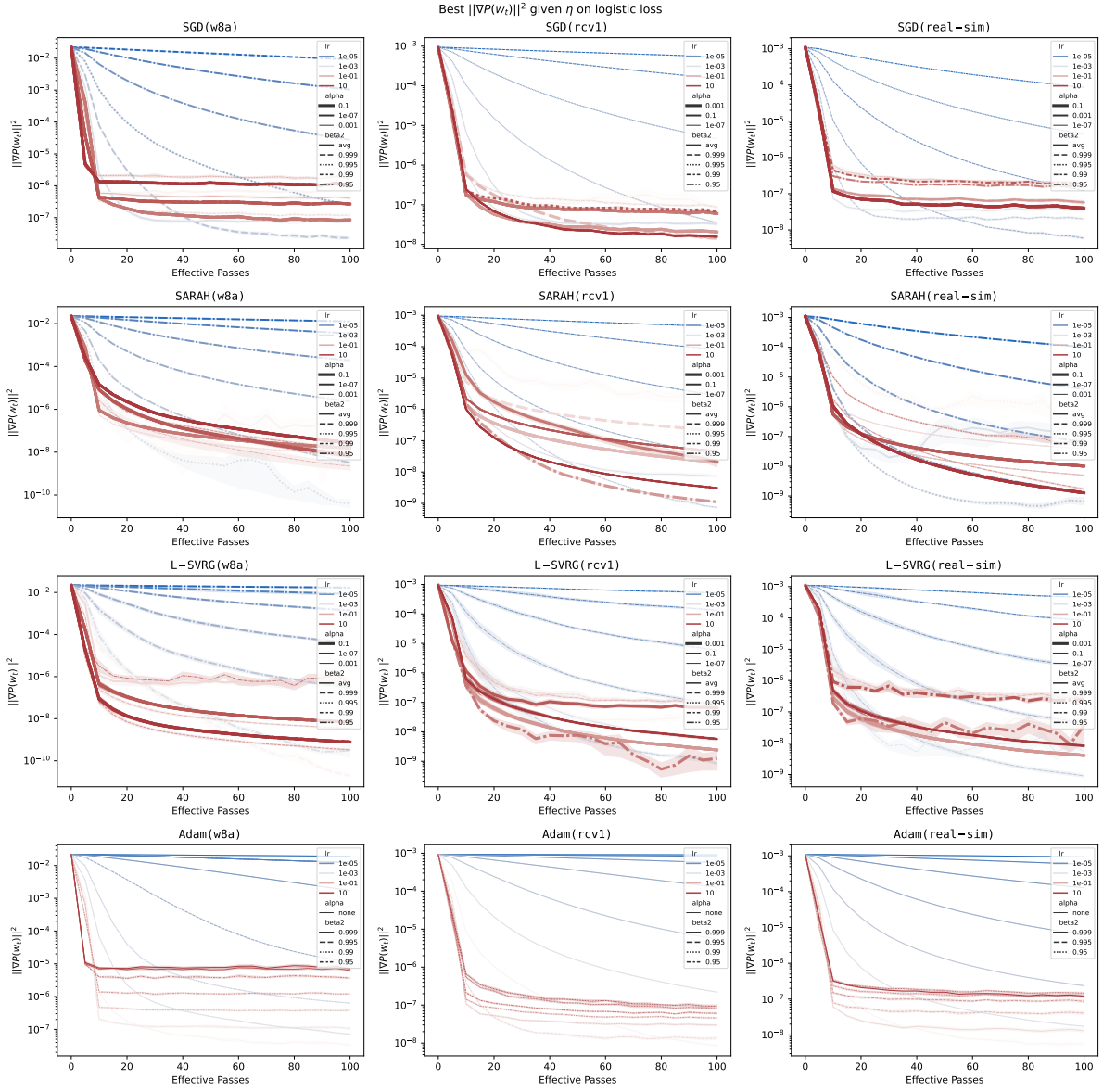


Figure 4: Trajectory of $\|\nabla P(w_t)\|^2$ of the best parameters minimizing the error given η and logistic loss.

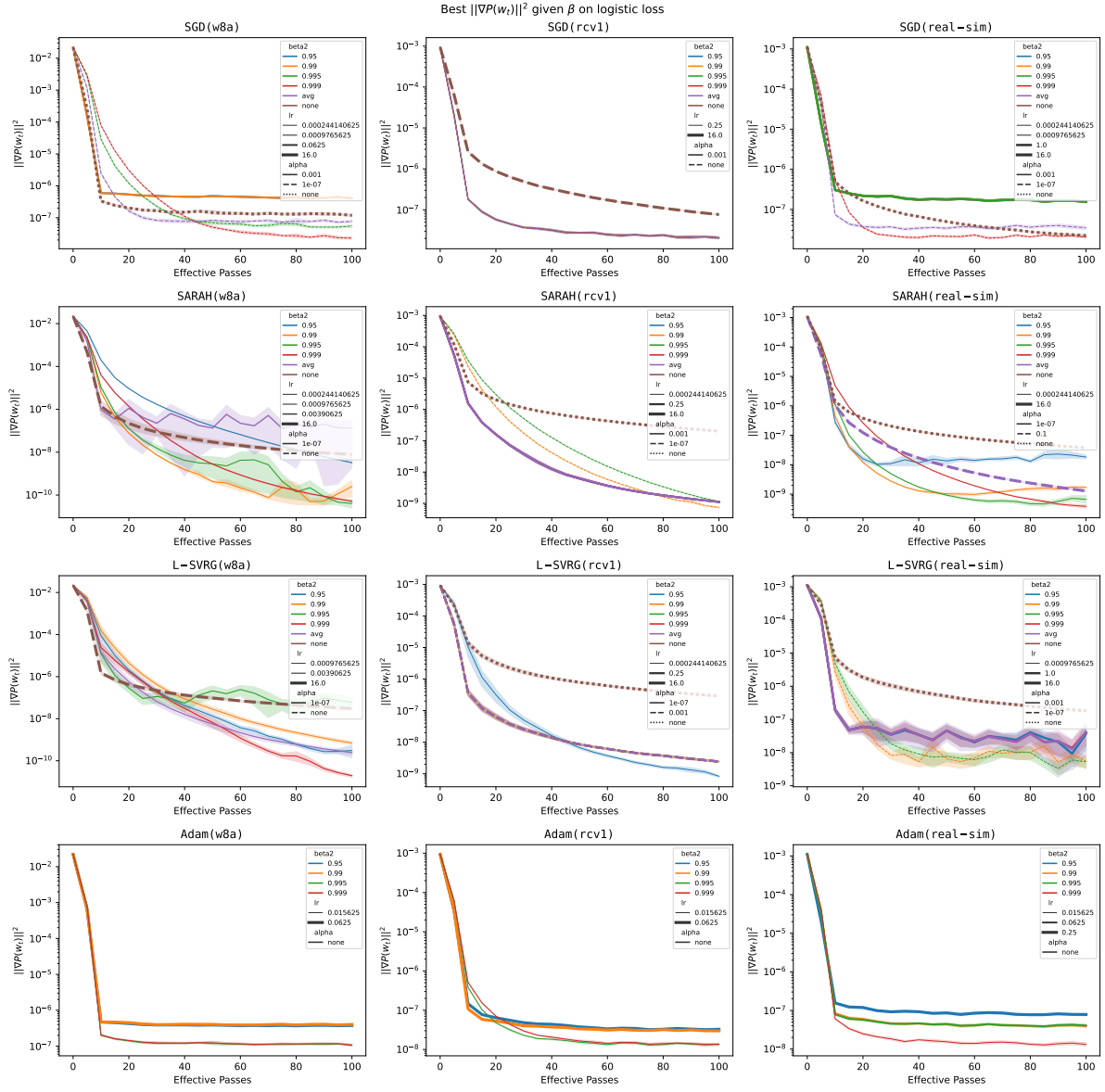


Figure 5: Trajectory of $\|\nabla P(w_t)\|^2$ of the best parameters minimizing the errors given β and logistic loss.

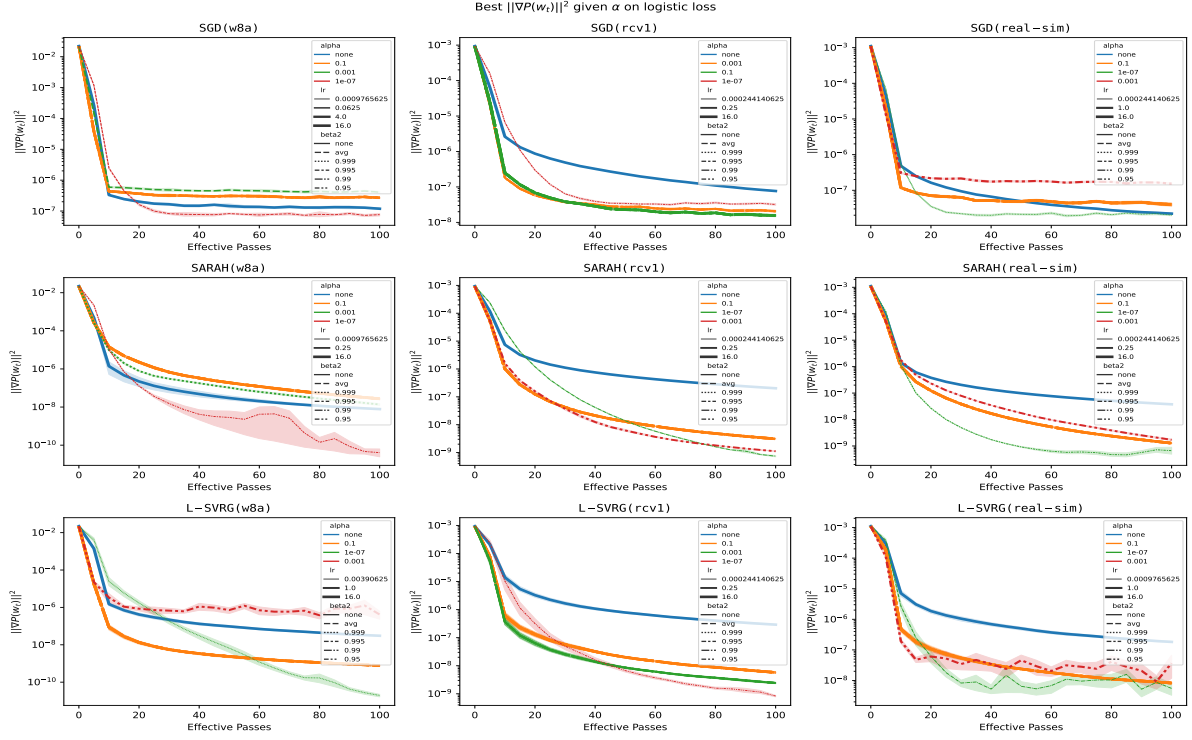


Figure 6: Trajectory of $\|\nabla P(w_t)\|^2$ of the best parameters minimizing the error given α and logistic loss.

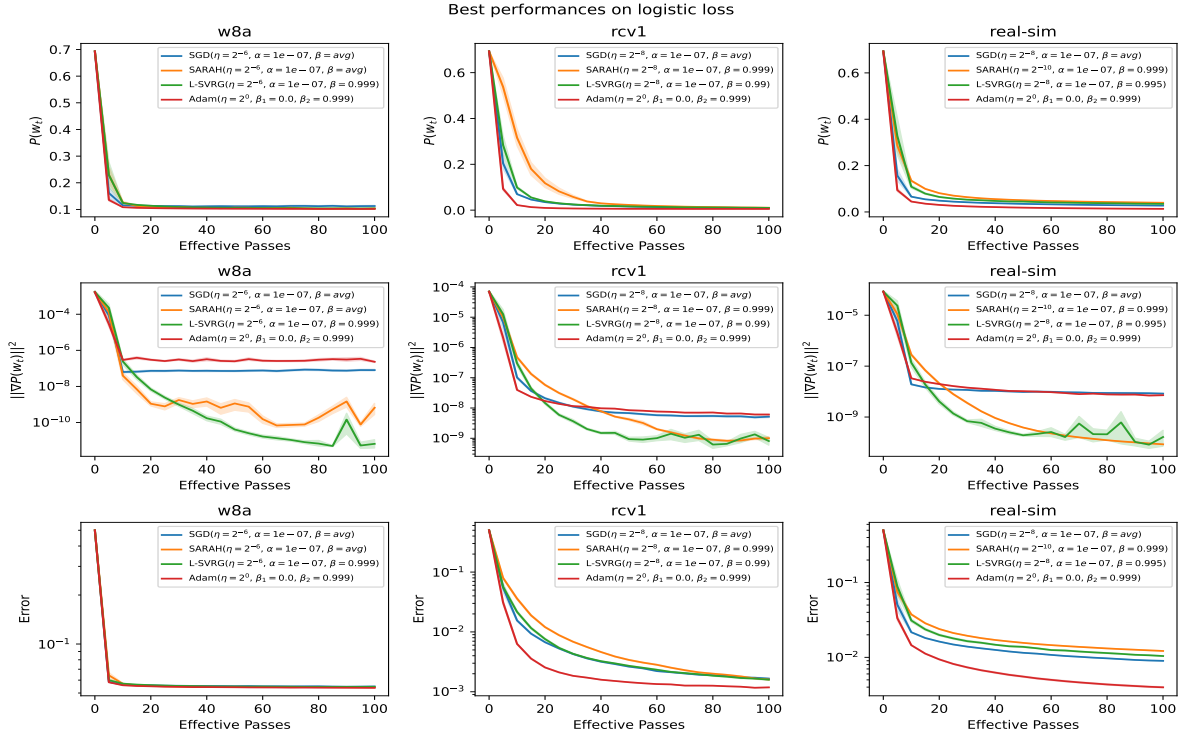


Figure 7: Performance of the best parameters minimizing the error given $(k_{min}, k_{max}) = (-3, 0)$.

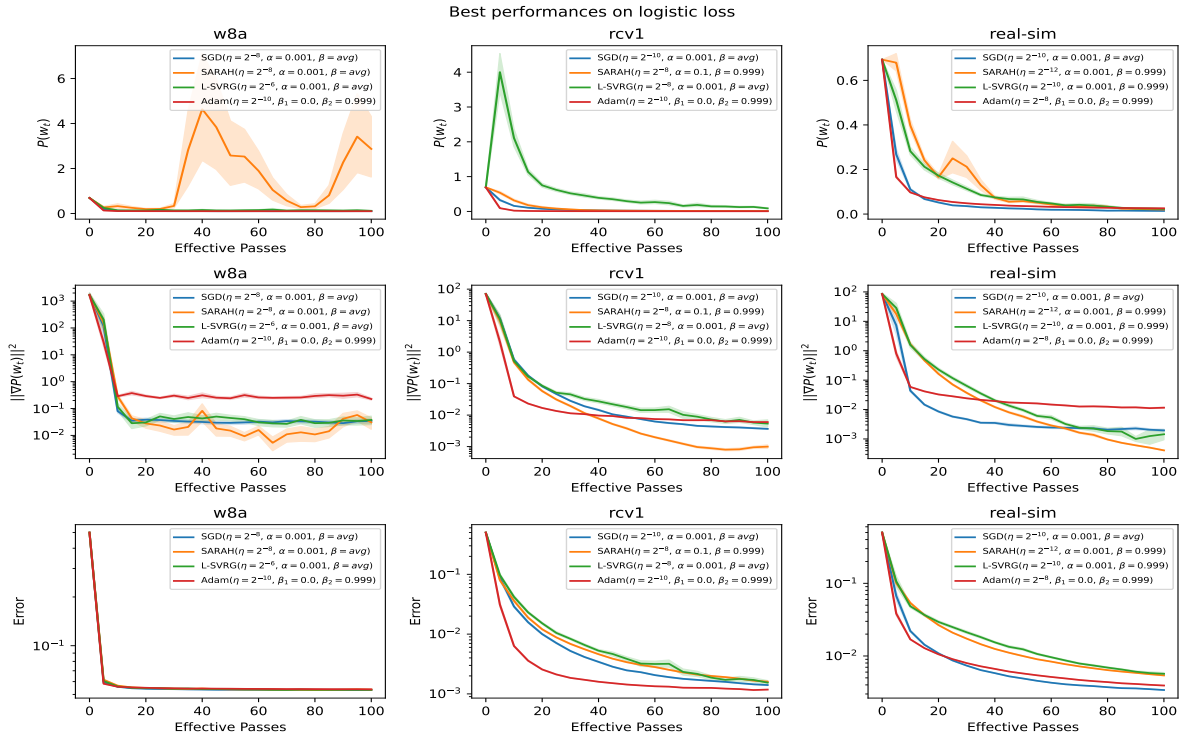


Figure 8: Performance of the best parameters minimizing the error given $(k_{min}, k_{max}) = (0, 3)$.

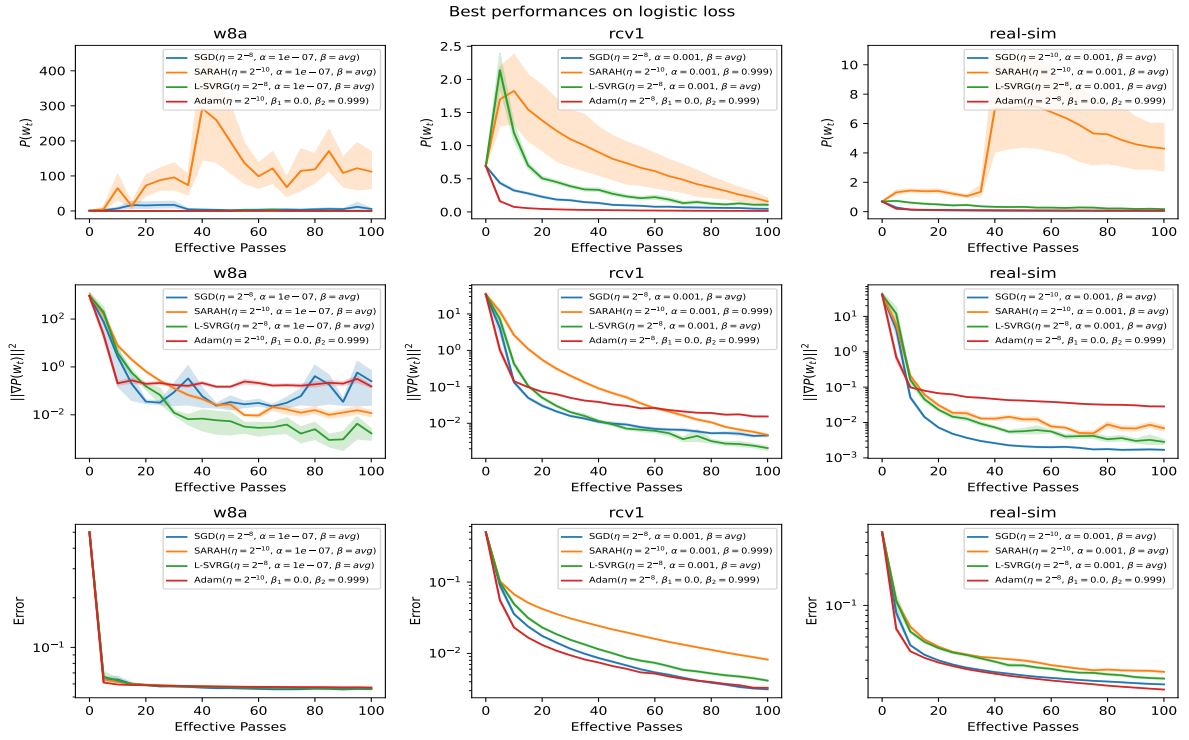


Figure 9: Performance of the best parameters minimizing the error given $(k_{min}, k_{max}) = (-3, 3)$.

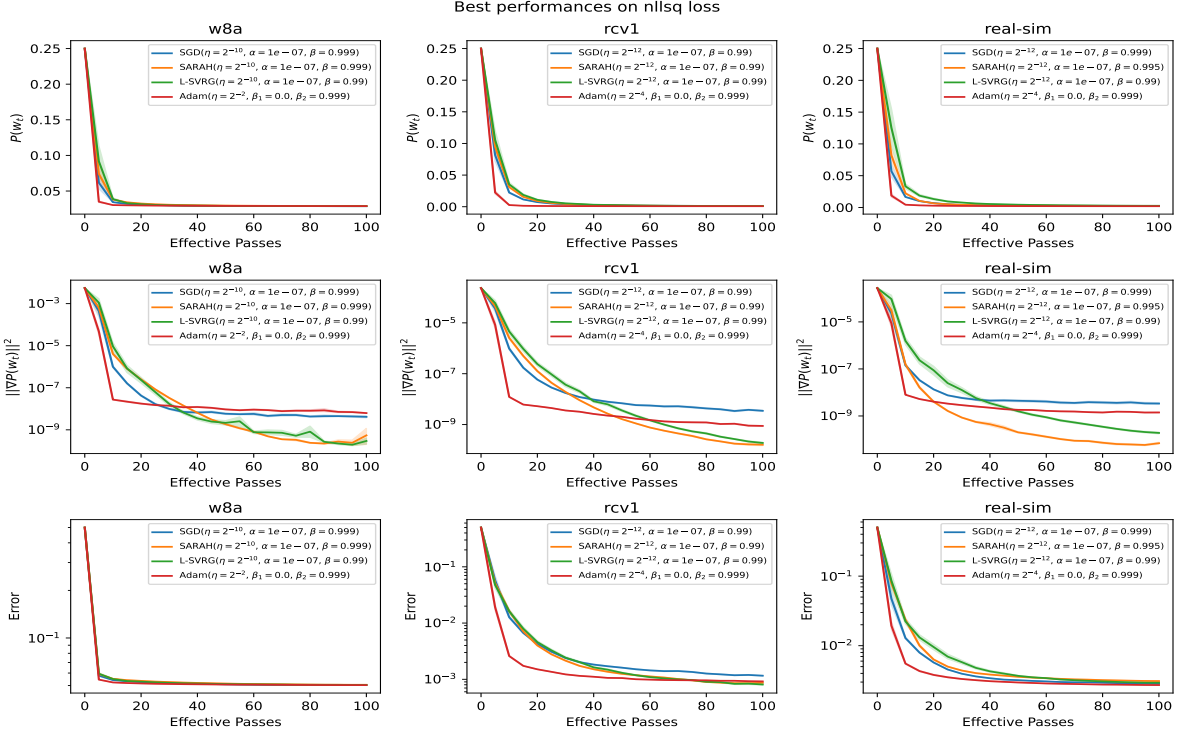


Figure 10: Performance of the best parameters minimizing the error using the NLLSQ loss.

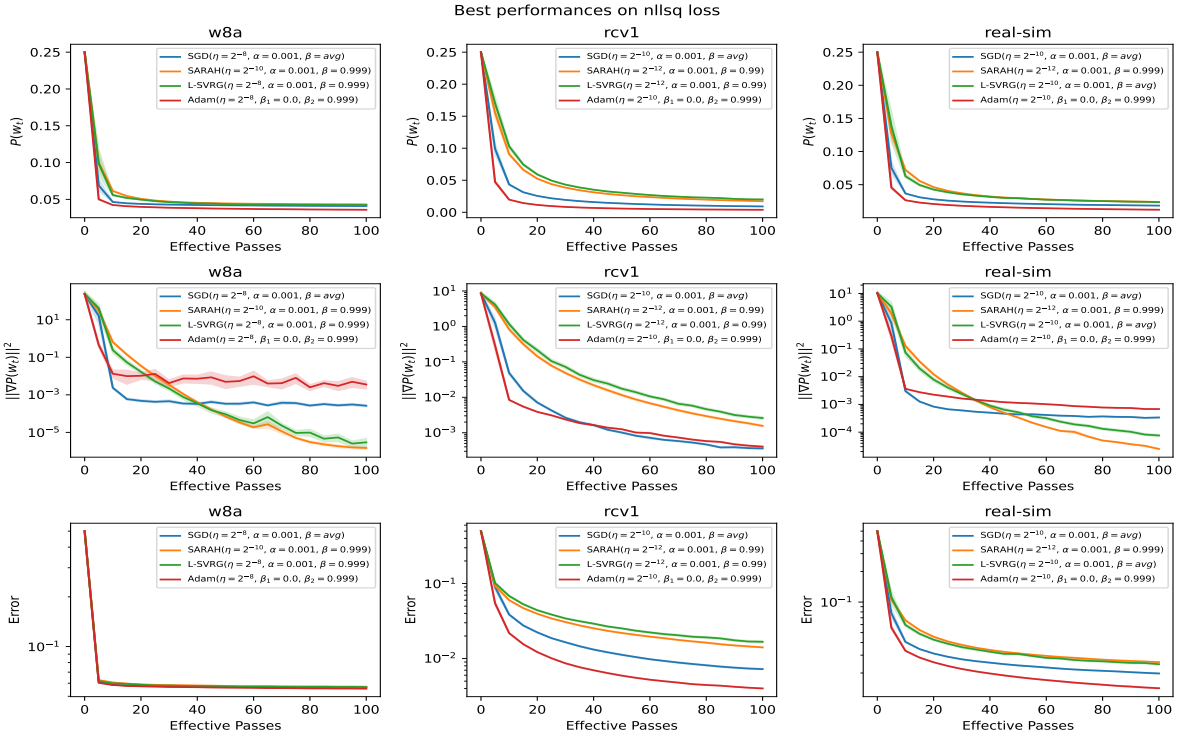


Figure 11: Performance of the best parameters minimizing the error on NLLSQ loss given $(k_{min}, k_{max}) = (-3, 3)$.

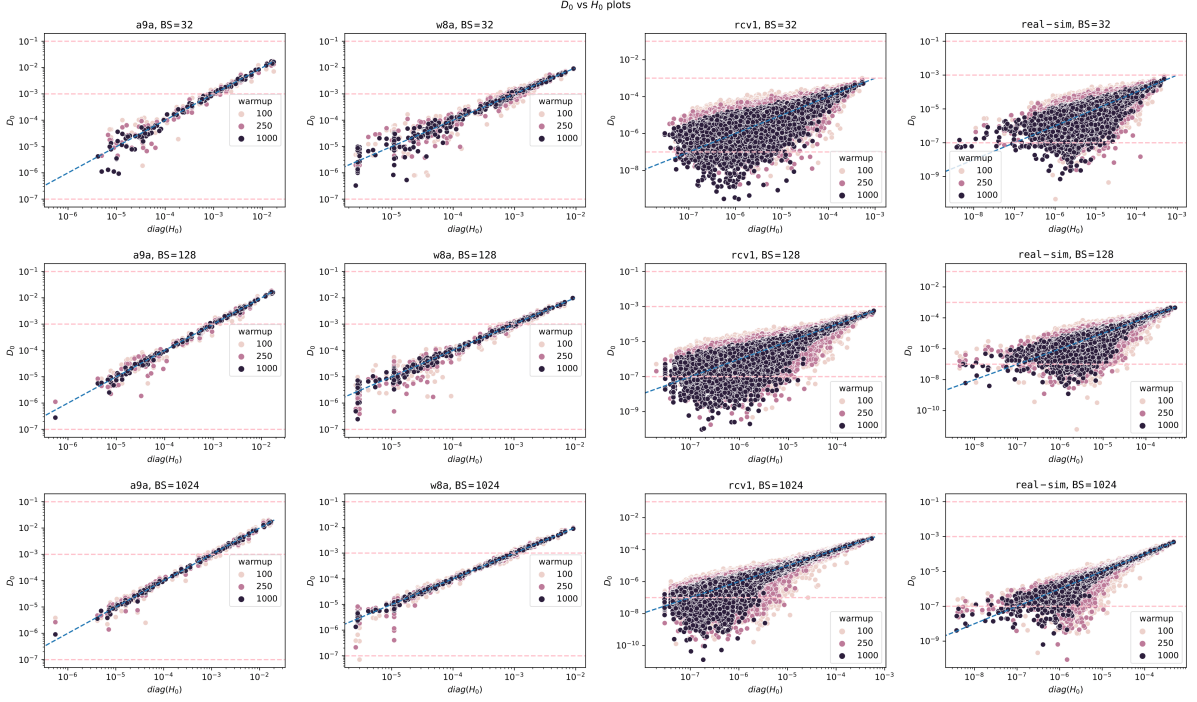


Figure 12: The diagonal values of the true hessian H_0 vs. the estimate D_0 . The tree α levels in our hyperparameter search grid are shown in a dashed pink horizontal lines. Increasing the number of warmup samples is beneficial, with slightly diminishing benefits as the batch size decreases. This can be seen from the larger number of light pink points around the diagonal for batch size 1024 on *real-sim*.

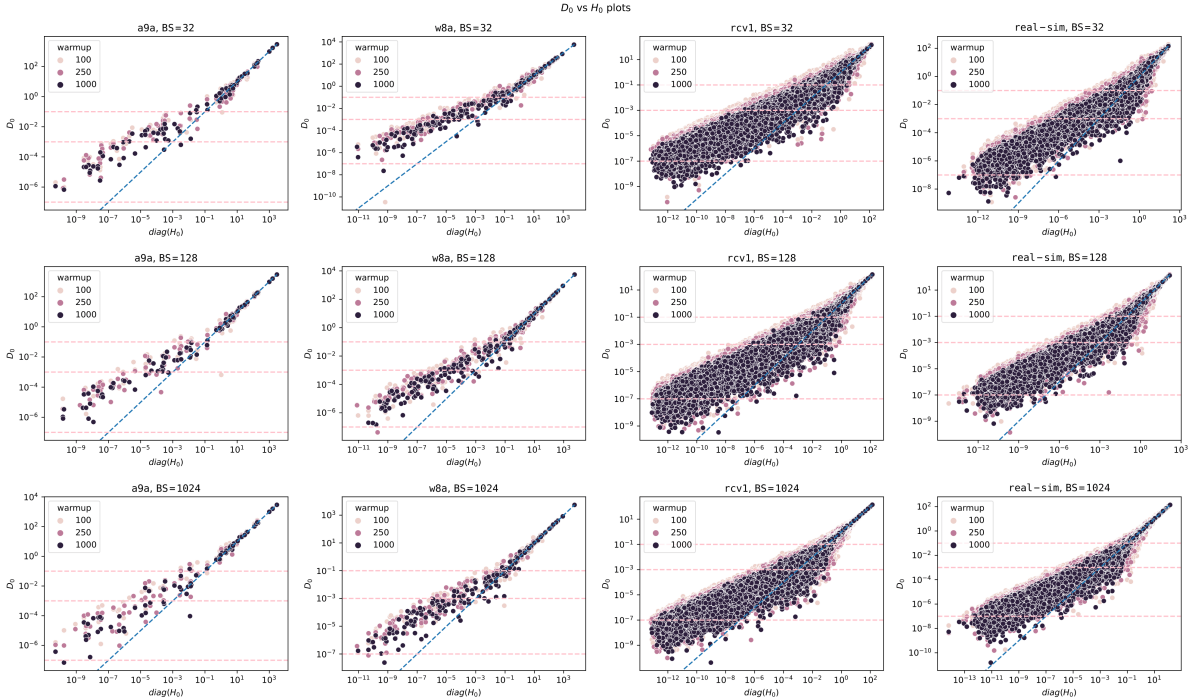


Figure 13: The diagonal values of the true hessian H_0 vs. the estimate D_0 given $(k_{min}, k_{max}) = (-3, 3)$.

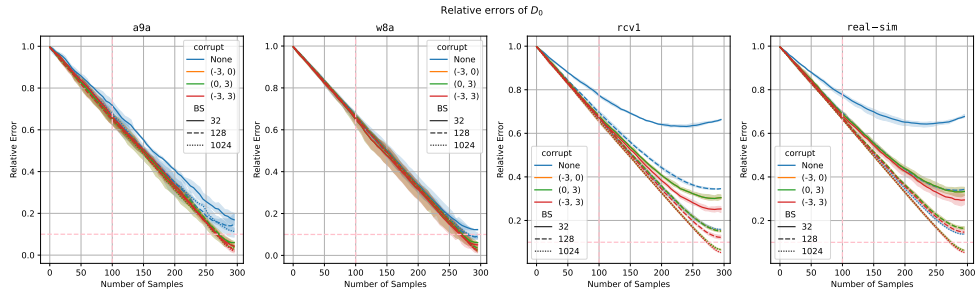


Figure 14: The relative error of the diagonal with respect to the diagonal of the true Hessian plotted against the number of warmup samples. The value `corrupt` indicates the feature scaling. For sparse datasets, it is more difficult to decrease the relative error below 0.1.

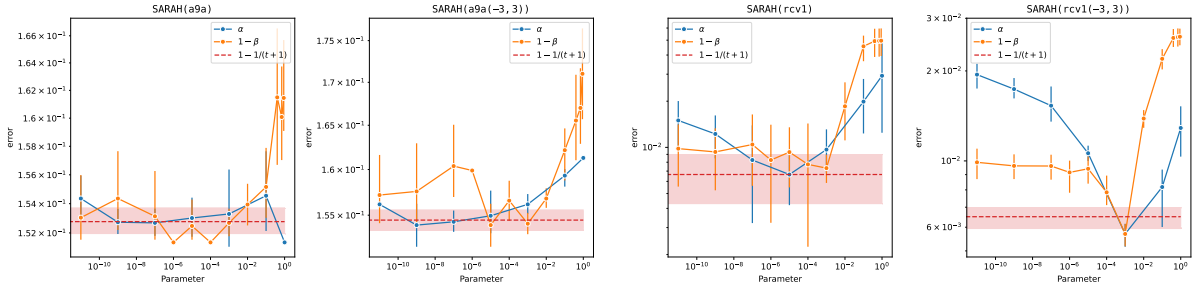


Figure 15: Optimal error achieved with the logistic loss given the value of the parameter. The optimal error for the "averaging" β_t is shown as a dashed red line. The arguments after the dataset name are the scaling factors.

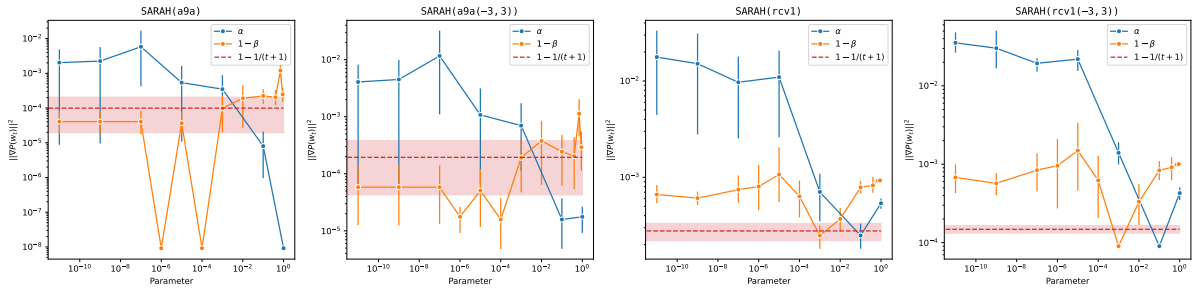


Figure 16: Optimal gradient norm achieved with the logistic loss given the value of the parameter. The optimal gradient norm for the "averaging" β_t is shown as a dashed red line. The arguments after the dataset name are the scaling factors.

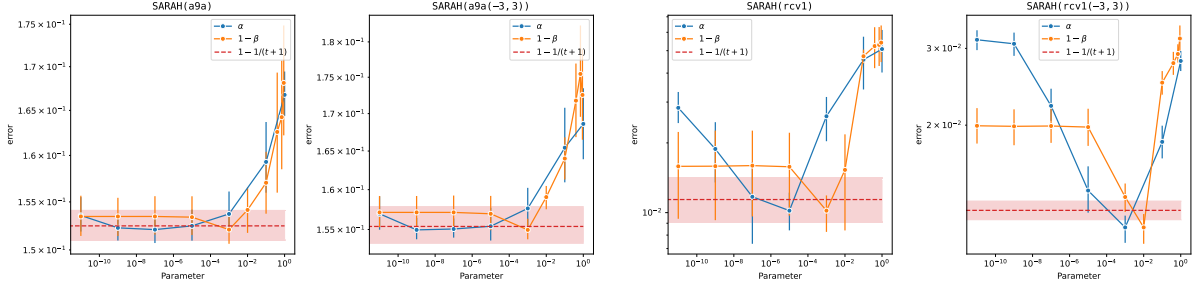


Figure 17: Optimal error achieved with the NLLSQ loss given the value of the parameter. The optimal error for the "averaging" β_t is shown as a dashed red line. The arguments after the dataset name are the scaling factors.

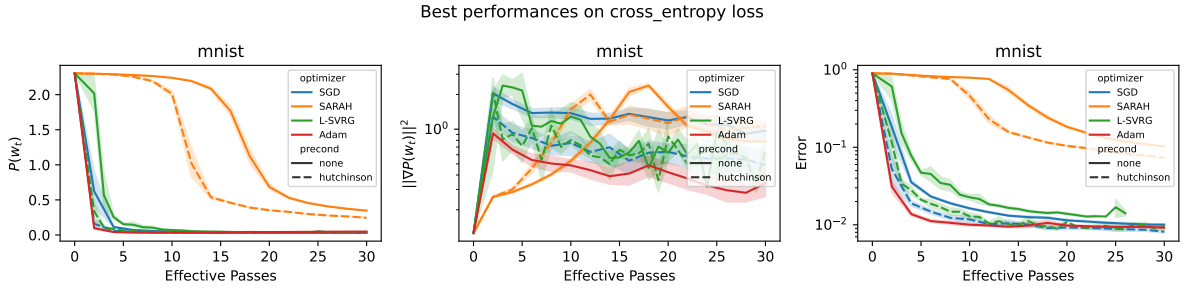


Figure 18: Best performances on MNIST vs. effective passes.

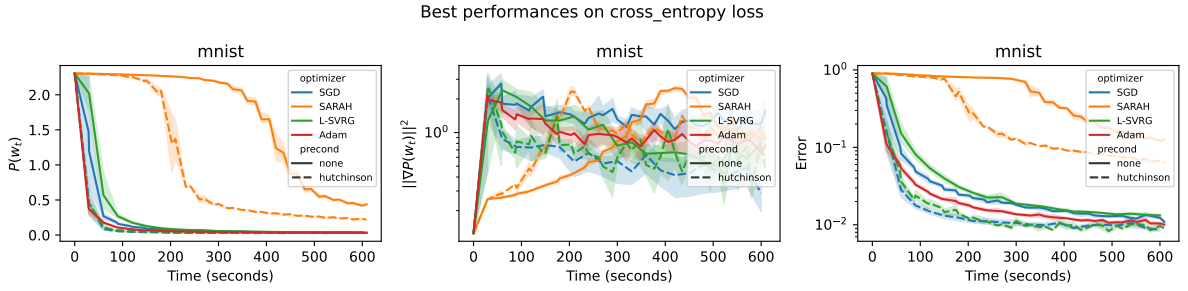


Figure 19: Best performances on MNIST vs. wall time in seconds.

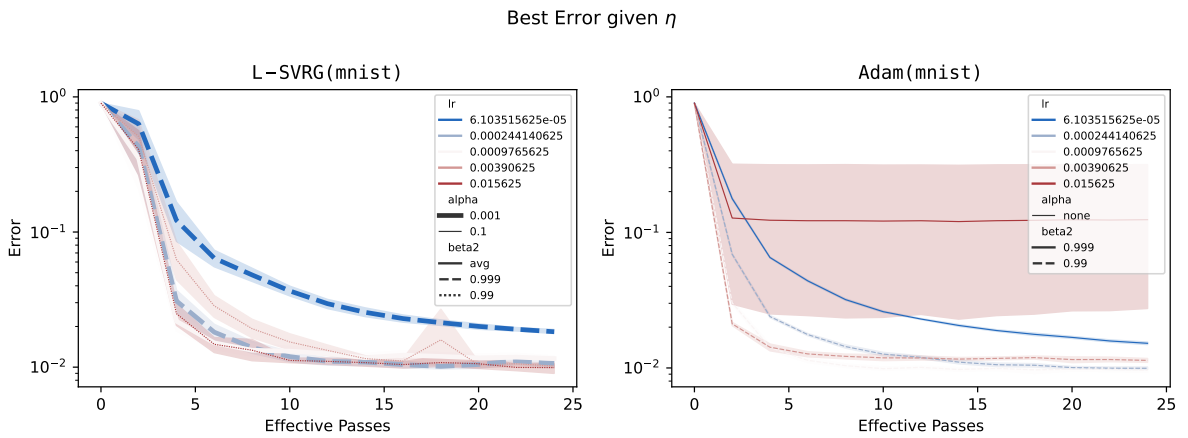


Figure 20: Best error given η on MNIST.

B Lemma 1

In this section we prove Lemma 1.

Proof. To begin, note that by constructing matrices \hat{D}_t according to (4) – (7), \hat{D}_t is a diagonal matrix with positive elements on the diagonal, where every elements is at least α . Hence, $\alpha I \preceq \hat{D}_t$.

To prove that $\hat{D}_t \preceq \Gamma I$, let us show that all elements of \hat{D}_t do not exceed Γ . Based on (4), it suffices to show that $\|\text{diag}(z_t \odot \nabla^2 P_{\mathcal{J}_t}(w_t) z_t)\|_\infty \leq \Gamma$ for all t .

$$\begin{aligned} \|\text{diag}(z_t \odot \nabla^2 P_{\mathcal{J}_t}(w_t) z_t)\|_\infty^2 &\leq \|z_t \odot \nabla^2 P_{\mathcal{J}_t}(w_t) z_t\|_\infty^2 \\ &\leq \left(\max_i \left[\sum_{j=1}^d |(\nabla^2 P_{\mathcal{J}_t}(w_t))_{ij}| \right] \right)^2 \leq \max_i \left(\sum_{j=1}^d |(\nabla^2 P_{\mathcal{J}_t}(w_t))_{ij}| \right)^2 \\ &\leq \max_i \left[d \sum_{j=1}^d (\nabla^2 P_{\mathcal{J}_t}(w_t))_{ij}^2 \right] \leq d \sum_{i=1}^d \sum_{j=1}^d (\nabla^2 P_{\mathcal{J}_t}(w_t))_{ij}^2 \\ &\leq d \|\nabla^2 P_{\mathcal{J}_t}(w_t)\|_2^2 \leq dL^2. \end{aligned}$$

In the last step we use L -smoothness of f_i (Assumption 1). Finally, we have

$$\|\text{diag}(z_t \odot \nabla^2 P_{\mathcal{J}_t}(w_t) z_t)\|_\infty \leq \sqrt{d}L = \Gamma.$$

□

C Lemma 1 for Adam

In this section we prove Lemma 1, but for Adam preconditioning. The rules for calculating the \hat{D} -matrix for Adam method are as follows:

$$D_t^2 = \beta_t D_{t-1}^2 + (1 - \beta_t) H_{\mathcal{J}_t}^2, \quad D_0^2 = \frac{1}{|\mathcal{J}_0|} \sum_{j \in \mathcal{J}_0} \text{diag}(\nabla f_j(w_0) \odot \nabla f_j(w_0))$$

where

$$\beta_t = \frac{\beta - \beta^{t+1}}{1 - \beta^{t+1}} \quad \text{with} \quad \beta \in (0; 1), \quad H_{\mathcal{J}_t}^2 = \frac{1}{|\mathcal{J}_t|} \sum_{j \in \mathcal{J}_t} \text{diag}(\nabla f_j(w_t) \odot \nabla f_j(w_t)),$$

and

$$\left(\hat{D}_t \right)_{i,i} = \max\{\alpha, |D_t|_{i,i}\}.$$

Lemma 2. For any $t \geq 1$, we have $\alpha I \preceq \hat{D}_t \preceq \Gamma I$, where $0 < \alpha \leq \Gamma = M$.

Proof. To begin, note that by constructing matrices \hat{D}_t according to these rules, \hat{D}_t is a diagonal matrix with positive elements on the diagonal, where every elements is at least α . Hence,

$\alpha I \preceq \hat{D}_t$. Moreover, using the diagonal structure of $H_{\mathcal{J}_t}^2$, one can note that

$$\begin{aligned}
\|H_{\mathcal{J}_t}^2\|_\infty &= \left\| \frac{1}{|\mathcal{J}_t|} \sum_{j \in \mathcal{J}_t} \text{diag}(\nabla f_j(w_t) \odot \nabla f_j(w_t)) \right\|_\infty \\
&\leq \frac{1}{|\mathcal{J}_t|} \sum_{j \in \mathcal{J}_t} \|\text{diag}(\nabla f_j(w_t) \odot \nabla f_j(w_t))\|_\infty \\
&= \frac{1}{|\mathcal{J}_t|} \sum_{j \in \mathcal{J}_t} \|\nabla f_j(w_t) \odot \nabla f_j(w_t)\|_\infty \\
&= \frac{1}{|\mathcal{J}_t|} \sum_{j \in \mathcal{J}_t} \|\nabla f_j(w_t)\|_\infty^2 \\
&\leq \frac{1}{|\mathcal{J}_t|} \sum_{j \in \mathcal{J}_t} \|\nabla f_j(w_t)\|_2^2 \leq M^2.
\end{aligned}$$

Finally, we have $\|H_{\mathcal{J}_t}^2\|_\infty \leq M^2$. And then, $\alpha I \preceq \hat{D}_t \preceq MI = \Gamma I$. \square

D Scaled SARAH

In this section we present the proofs for the main theoretical complexity results for the **Scaled SARAH** from Section 3.

Lemma 3 (Descent Lemma). Suppose that function P satisfies Assumption 1 and Algorithm 1 generate a sequence $\{w_t\}_{t \geq 0}$. Then we have for any $t \geq 0$ and η

$$P(w_{t+1}) \leq P(w_t) + \frac{\eta}{2\alpha} \|\nabla P(w_t) - v_t\|^2 - \left(\frac{1}{2\eta} - \frac{L}{2\alpha} \right) \|w_{t+1} - w_t\|_{\hat{D}_t}^2 - \frac{\eta}{2} \|\nabla P(w_t)\|_{\hat{D}_t^{-1}}^2.$$

Proof. Using L -smoothness of the function P and $I \preceq \frac{1}{\alpha} \hat{D}_t$

$$\begin{aligned}
P(w_{t+1}) &\leq P(w_t) + \langle \nabla P(w_t), w_{t+1} - w_t \rangle + \frac{L}{2} \|w_{t+1} - w_t\|^2 \\
&\leq P(w_t) + \langle \nabla P(w_t), w_{t+1} - w_t \rangle + \frac{L}{2\alpha} \|w_{t+1} - w_t\|_{\hat{D}_t}^2.
\end{aligned}$$

With an update of **Scaled SARAH**: $w_{t+1} = w_t - \eta \hat{D}_t^{-1} v_t$, we get

$$\begin{aligned}
P(w_{t+1}) &\leq P(w_t) + \langle \nabla P(w_t) - v_t, -\eta \hat{D}_t^{-1} v_t \rangle + \frac{1}{\eta} \langle \hat{D}_t (w_t - w_{t+1}), w_{t+1} - w_t \rangle \\
&\quad + \frac{L}{2\alpha} \|w_{t+1} - w_t\|_{\hat{D}_t}^2 \\
&= P(w_t) + \eta \langle \nabla P(w_t) - v_t, \nabla P(w_t) - v_t \rangle_{\hat{D}_t^{-1}} \\
&\quad - \eta \langle \nabla P(w_t) - v_t, \nabla P(w_t) \rangle_{\hat{D}_t^{-1}} - \left(\frac{1}{\eta} - \frac{L}{2\alpha} \right) \|w_{t+1} - w_t\|_{\hat{D}_t}^2 \\
&= P(w_t) + \eta \|\nabla P(w_t) - v_t\|_{\hat{D}_t^{-1}}^2 - \eta \langle \nabla P(w_t) - v_t, \nabla P(w_t) \rangle_{\hat{D}_t^{-1}} \\
&\quad - \left(\frac{1}{\eta} - \frac{L}{2\alpha} \right) \|w_{t+1} - w_t\|_{\hat{D}_t}^2.
\end{aligned}$$

Let us define $\bar{w}_{t+1} = w_t - \eta \hat{D}_t^{-1} \nabla P(w_t)$. Using this new notation and an update $w_{t+1} = w_t - \eta \hat{D}_t^{-1} v_t$, then we have

$$\begin{aligned}
P(w_{t+1}) &\leq P(w_t) + \eta \|\nabla P(w_t) - v_t\|_{\hat{D}_t^{-1}}^2 - \frac{1}{\eta} \langle w_{t+1} - \bar{w}_{t+1}, w_t - \bar{w}_{t+1} \rangle_{\hat{D}_t} \\
&\quad - \left(\frac{1}{\eta} - \frac{L}{2\alpha} \right) \|w_{t+1} - w_t\|_{\hat{D}_t}^2 \\
&= P(w_t) + \eta \|\nabla P(w_t) - v_t\|_{\hat{D}_t^{-1}}^2 - \left(\frac{1}{\eta} - \frac{L}{2\alpha} \right) \|w_{t+1} - w_t\|_{\hat{D}_t}^2 \\
&\quad - \frac{1}{2\eta} \left(\|w_{t+1} - \bar{w}_{t+1}\|_{\hat{D}_t}^2 + \|w_t - \bar{w}_{t+1}\|_{\hat{D}_t}^2 - \|w_{t+1} - w_t\|_{\hat{D}_t}^2 \right) \\
&= P(w_t) + \eta \|\nabla P(w_t) - v_t\|_{\hat{D}_t^{-1}}^2 - \left(\frac{1}{\eta} - \frac{L}{2\alpha} \right) \|w_{t+1} - w_t\|_{\hat{D}_t}^2 \\
&\quad - \frac{1}{2\eta} \left(\eta^2 \|\nabla P(w_t) - v_t\|_{\hat{D}_t^{-1}}^2 + \eta^2 \|\nabla P(w_t)\|_{\hat{D}_t^{-1}}^2 - \|w_{t+1} - w_t\|_{\hat{D}_t}^2 \right).
\end{aligned}$$

□

Lemma 4. Suppose that the function P satisfies Assumptions 1, 2 and Algorithm 1 generate a sequence $\{w_t\}_{t \geq 0}$. Then we have for any $t \geq 0$ and η

$$P(w_{t+1}) - P^* \leq \left(1 - \frac{\eta\mu}{\Gamma}\right) (P(w_t) - P^*) + \frac{\eta}{2\alpha} \|\nabla P(w_t) - v_t\|^2 - \left(\frac{1}{2\eta} - \frac{L}{2\alpha}\right) \|w_{t+1} - w_t\|_{\hat{D}_t}^2. \quad (11)$$

Proof. According Lemma 3, we have

$$P(w_{t+1}) \leq P(w_t) + \frac{\eta}{2\alpha} \|\nabla P(w_t) - v_t\|^2 - \left(\frac{1}{2\eta} - \frac{L}{2\alpha}\right) \|w_{t+1} - w_t\|_{\hat{D}_t}^2 - \frac{\eta}{2} \|\nabla P(w_t)\|_{\hat{D}_t^{-1}}^2.$$

Then with $\frac{1}{\Gamma} I \preceq \hat{D}_t^{-1}$ and PL-condition, we have

$$\begin{aligned}
P(w_{t+1}) - P^* &\leq P(w_t) - P^* + \frac{\eta}{2\alpha} \|\nabla P(w_t) - v_t\|^2 - \left(\frac{1}{2\eta} - \frac{L}{2\alpha}\right) \|w_{t+1} - w_t\|_{\hat{D}_t}^2 \\
&\quad - \frac{\eta}{2\Gamma} \|\nabla P(w_t)\|^2 \\
&\leq P(w_t) - P^* + \frac{\eta}{2\alpha} \|\nabla P(w_t) - v_t\|^2 - \left(\frac{1}{2\eta} - \frac{L}{2\alpha}\right) \|w_{t+1} - w_t\|_{\hat{D}_t}^2 \\
&\quad - \frac{\eta\mu}{\Gamma} (P(w_t) - P^*).
\end{aligned}$$

□

Lemma 5. Suppose that Assumption 1 holds. Then we have

$$\mathbb{E} [\|v_{t+1} - \nabla P(w_{t+1})\|^2] \leq (1-p) \mathbb{E} [\|v_t - \nabla P(w_t)\|^2] + \frac{(1-p)L^2}{\alpha} \mathbb{E} [\|w_{t+1} - w_t\|_{\hat{D}_t}^2].$$

Proof. Lemma 3 from [Li et al., 2021a] gives

$$\mathbb{E} [\|v_{t+1} - \nabla P(w_{t+1})\|^2] \leq (1-p) \mathbb{E} [\|v_t - \nabla P(w_t)\|^2] + (1-p)L^2 \mathbb{E} [\|w_{t+1} - w_t\|^2].$$

Using $I \preceq \frac{1}{\alpha} \hat{D}_t$, we get

$$\mathbb{E} [\|v_{t+1} - \nabla P(w_{t+1})\|^2] \leq (1-p)\mathbb{E} [\|v_t - \nabla P(w_t)\|^2] + \frac{(1-p)L^2}{\alpha} \mathbb{E} [\|w_{t+1} - w_t\|_{\hat{D}_t}^2].$$

□

Theorem 5 (Theorem 1). Suppose that Assumption 1 holds, let $\varepsilon > 0$, let p denote the probability, and let the step-size satisfy

$$\eta \leq \frac{\alpha}{L \left(1 + \sqrt{\frac{1-p}{p}}\right)}.$$

Then, the number of iterations performed by Scaled SARAH, starting from an initial point $w_0 \in \mathbb{R}^d$ with $\Delta_0 = P(w_0) - P^*$, required to obtain an ε -approximate solution of the non-convex finite-sum problem (1) can be bounded by

$$T = \mathcal{O} \left(\frac{\Gamma \Delta_0 L}{\alpha \varepsilon^2} \left(1 + \sqrt{\frac{1-p}{p}}\right) \right).$$

Proof. Using Lemmas 3, 5, we have

$$\begin{aligned} & \mathbb{E} \left[P(w_{t+1}) - P^* + \frac{\eta}{2\alpha p} \|\nabla P(w_{t+1}) - v_{t+1}\|^2 \right] \\ & \leq \mathbb{E} \left[P(w_t) - P^* + \frac{\eta}{2\alpha} \|\nabla P(w_t) - v_t\|^2 \right] \\ & \quad - \left(\frac{1}{2\eta} - \frac{L}{2\alpha} \right) \mathbb{E} [\|w_{t+1} - w_t\|_{\hat{D}_t}^2] - \frac{\eta}{2} \mathbb{E} [\|\nabla P(w_t)\|_{\hat{D}_t}^2] \\ & \quad + \frac{\eta}{2\alpha p} \left((1-p)\mathbb{E} [\|v_t - \nabla P(w_t)\|^2] + \frac{(1-p)L^2}{\alpha} \mathbb{E} [\|w_{t+1} - w_t\|_{\hat{D}_t}^2] \right) \\ & = \mathbb{E} \left[P(w_t) - P^* + \frac{\eta}{2\alpha p} \|\nabla P(w_t) - v_t\|^2 \right] - \frac{\eta}{2} \mathbb{E} [\|\nabla P(w_t)\|_{\hat{D}_t}^2] \\ & \quad - \left(\frac{1}{2\eta} - \frac{L}{2\alpha} - \frac{(1-p)L^2}{2\alpha^2 p} \eta \right) \mathbb{E} [\|w_{t+1} - w_t\|_{\hat{D}_t}^2]. \end{aligned}$$

Choosing $\eta \leq \frac{\alpha}{L(1+\sqrt{\frac{1-p}{p}})}$ and defining $\Psi_{t+1} = P(w_{t+1}) - P^* + \frac{\eta}{2\alpha p} \|\nabla P(w_{t+1}) - v_{t+1}\|^2$, we have

$$\mathbb{E} [\Psi_{t+1}] \leq \mathbb{E} [\Psi_t] - \frac{\eta}{2} \mathbb{E} [\|\nabla P(w_t)\|_{\hat{D}_t}^2].$$

Summing up, we obtain

$$\sum_{t=0}^{T-1} \frac{\eta}{2} \mathbb{E} [\|\nabla P(w_t)\|_{\hat{D}_t}^2] \leq \mathbb{E} [\Psi_0] - \mathbb{E} [\Psi_T].$$

Using that \hat{w}_T is chosen uniformly from all w_t from 0 to $T-1$, we have

$$\frac{\eta}{2} \mathbb{E} [\|\nabla P(\hat{w}_T)\|_{\hat{D}_T}^2] \leq \frac{\mathbb{E} [\Psi_0] - \mathbb{E} [\Psi_T]}{T}.$$

With $\Delta_0 = \Psi_0 = P(w_0) - P^*$, we get

$$\mathbb{E} \|\nabla P(\hat{w}_T)\|^2 \leq \Gamma \mathbb{E} \|\nabla P(\hat{w}_T)\|_{\hat{D}_T}^2 \leq \frac{2\Delta_0 \Gamma}{\eta T}.$$

Then

$$T = \mathcal{O}\left(\frac{\Delta_0 \Gamma}{\eta \varepsilon^2}\right) = \mathcal{O}\left(\frac{L \Delta_0 \Gamma}{\varepsilon^2 \alpha} \left(1 + \sqrt{\frac{1-p}{p}}\right)\right).$$

□

Theorem 6 (Theorem 2). Suppose that Assumptions 1 and 2 hold, let $\varepsilon > 0$, and let the step-size satisfy

$$\eta \leq \frac{\alpha}{L \left(1 + \sqrt{\frac{1-p}{p}}\right)}.$$

Then the number of iterations performed by Scaled SARAH sufficient for finding an ε -approximate solution of non-convex finite-sum problem (1) can be bounded by

$$T = \mathcal{O}\left(\max\left\{\frac{1}{p}, \frac{L \Gamma}{\mu \alpha} \left(1 + \sqrt{\frac{1-p}{p}}\right)\right\} \log \frac{\Delta_0}{\varepsilon}\right).$$

Proof. Using Lemmas 4, 5, we have for some $B > 0$

$$\begin{aligned} & \mathbb{E}\left[P(w_{t+1}) - P^* + B\|\nabla P(w_{t+1}) - v_{t+1}\|^2\right] \\ & \leq \left(1 - \frac{\eta\mu}{\Gamma}\right) \mathbb{E}[P(w_t) - P^*] + \frac{\eta}{2\alpha} \mathbb{E}[\|\nabla P(w_t) - v_t\|^2] \\ & \quad - \left(\frac{1}{2\eta} - \frac{L}{2\alpha}\right) \mathbb{E}\left[\|w_{t+1} - w_t\|_{\hat{D}_t}^2\right] \\ & \quad + B \left((1-p) \mathbb{E}[\|v_t - \nabla P(w_t)\|^2] + \frac{(1-p)L^2}{\alpha} \mathbb{E}\left[\|w_{t+1} - w_t\|_{\hat{D}_t}^2\right] \right) \\ & \leq \left(1 - \frac{\eta\mu}{\Gamma}\right) \mathbb{E}[P(w_t) - P^*] + \left(\frac{\eta}{2\alpha} + B(1-p)\right) \mathbb{E}[\|\nabla P(w_t) - v_t\|^2] \\ & \quad - \left(\frac{1}{2\eta} - \frac{L}{2\alpha} - \frac{(1-p)L^2}{\alpha} B\right) \mathbb{E}\left[\|w_{t+1} - w_t\|_{\hat{D}_t}^2\right]. \end{aligned}$$

We need to choose η, B such that

$$\frac{\eta}{2\alpha} + B(1-p) \leq \left(1 - \frac{\eta\mu}{\Gamma}\right) B; \quad \frac{1}{2\eta} - \frac{L}{2\alpha} - \frac{(1-p)L^2}{\alpha} B \geq 0.$$

If we take $B = \frac{\eta}{p\alpha}$ and $\eta \leq \min\left\{\frac{p\Gamma}{2\mu}, \frac{\alpha}{2L(1+\sqrt{\frac{1-p}{p}})}\right\}$, we get

$$\begin{aligned} & \mathbb{E}\left[P(w_{t+1}) - P^* + B\|\nabla P(w_{t+1}) - v_{t+1}\|^2\right] \\ & \leq \left(1 - \frac{\eta\mu}{\Gamma}\right) \mathbb{E}\left[P(w_t) - P^* + B\|\nabla P(w_t) - v_t\|^2\right]. \end{aligned}$$

and then obtain

$$\mathbb{E}[P(w_T) - P^*] \leq \mathbb{E}\left[P(w_T) - P^* + B\|\nabla P(w_T) - v_T\|^2\right] \leq \left(1 - \frac{\eta\mu}{\Gamma}\right)^T \Delta_0.$$

Finally, to achieve ε -approximate solution ($\mathbb{E}[P(w_T) - P^*] \leq \varepsilon$), we need

$$T = \mathcal{O}\left(\frac{\Gamma}{\eta\mu} \log \frac{\Delta_0}{\varepsilon}\right) = \mathcal{O}\left(\max\left\{\frac{1}{p}, \frac{L \Gamma}{\mu \alpha} \left(1 + \sqrt{\frac{1-p}{p}}\right)\right\} \log \frac{\Delta_0}{\varepsilon}\right) \text{ iterations.}$$

□

E Scaled L-SVRG

Here we provide proofs for our theoretical results for Scaled L-SVRG.

Lemma 6. Suppose that Algorithm 2 generate sequences $\{w_t\}_{t \geq 0}$ and $\{z_t\}_{t \geq 0}$. Then we have for any $t \geq 0$, any η and $B > 0$

$$\begin{aligned} \mathbb{E} [\|w_{t+1} - z_{t+1}\|^2] &\leq \frac{\eta^2}{\alpha} \mathbb{E} [\|v_t\|_{\hat{D}_t^{-1}}^2] + (1-p)(1+\eta B) \mathbb{E} [\|w_t - z_t\|^2] \\ &\quad + (1-p) \frac{\eta}{\alpha B} \mathbb{E} [\|\nabla P(w_t)\|_{\hat{D}_t^{-1}}^2]. \end{aligned}$$

Proof. Using definition z_{t+1} and an update of Scaled L-SVRG: $w_{t+1} = w_t - \eta \hat{D}_t^{-1} v_t$, we have

$$\begin{aligned} \mathbb{E} [\mathbb{E}_{z_{t+1}} [\|w_{t+1} - z_{t+1}\|^2]] &= p \mathbb{E} [\|w_{t+1} - w_t\|^2] + (1-p) \mathbb{E} [\|w_{t+1} - z_t\|^2] \\ &\leq \frac{p\eta^2}{\alpha} \mathbb{E} [\|v_t\|_{\hat{D}_t^{-1}}^2] + (1-p) \mathbb{E} [\|w_{t+1} - z_t\|^2]. \end{aligned} \quad (12)$$

In the last of the previous estimate, we used $\hat{D}_t^{-1} \preceq \frac{1}{\alpha} I$. Next, we estimate $\mathbb{E} [\|w_{t+1} - z_t\|^2]$:

$$\begin{aligned} \mathbb{E} [\|w_{t+1} - z_t\|^2] &= \mathbb{E} [\|w_t - \eta \hat{D}_t^{-1} v_t - z_t\|^2] \\ &\leq \mathbb{E} [\|w_t - z_t\|^2] + \frac{\eta^2}{\alpha} \mathbb{E} [\|v_t\|_{\hat{D}_t^{-1}}^2] - 2\eta \mathbb{E} [\langle \hat{D}_t^{-1} v_t, w_t - z_t \rangle]. \end{aligned}$$

Due to the fact that i_t and \mathcal{J}_{t-1} are generated uniformly and independently, we have that $\mathbb{E}_{i_t}[v_t] = \mathbb{E}_{i_t}[\nabla f_{i_t}(w_t) - \nabla f_{i_t}(z_t)] + \nabla P(z_t) = \nabla P(w_t) - \nabla P(z_t) + \nabla P(z_t) = \nabla P(w_t)$ and $\mathbb{E} [\langle \hat{D}_t^{-1} v_t, w_t - z_t \rangle] = \mathbb{E} [\langle \hat{D}_t^{-1} \mathbb{E}_{i_t}[v_t], w_t - z_t \rangle]$. Using these facts, we get for some $B > 0$

$$\begin{aligned} \mathbb{E} [\|w_{t+1} - z_t\|^2] &= \mathbb{E} [\|w_t - z_t\|^2] + \frac{\eta^2}{\alpha} \mathbb{E} [\|v_t\|_{\hat{D}_t^{-1}}^2] - 2\eta \mathbb{E} [\langle \hat{D}_t^{-1} \nabla P(w_t), w_t - z_t \rangle] \\ &\leq \mathbb{E} [\|w_t - z_t\|^2] + \frac{\eta^2}{\alpha} \mathbb{E} [\|v_t\|_{\hat{D}_t^{-1}}^2] \\ &\quad + \eta \left(\frac{1}{\alpha B} \mathbb{E} [\|\nabla P(w_t)\|_{\hat{D}_t^{-1}}^2] + B \mathbb{E} [\|w_t - z_t\|^2] \right) \\ &= (1 + \eta B) \mathbb{E} [\|w_t - z_t\|^2] + \frac{\eta}{\alpha B} \mathbb{E} [\|\nabla P(w_t)\|_{\hat{D}_t^{-1}}^2] \\ &\quad + \frac{\eta^2}{\alpha} \mathbb{E} [\|v_t\|_{\hat{D}_t^{-1}}^2]. \end{aligned} \quad (13)$$

Combining (12) and (13), we finish proof. \square

Lemma 7. Suppose that function P satisfies Assumption 1 and Algorithm 2 generate a sequence $\{w_t\}_{t \geq 0}$. Then we have for any $t \geq 0$ and η

$$\mathbb{E} [\|v_t\|_{\hat{D}_t^{-1}}^2] \leq 3 \mathbb{E} [\|\nabla P(w_t)\|_{\hat{D}_t^{-1}}^2] + \frac{6L^2}{\alpha} \mathbb{E} [\|w_t - z_t\|^2]. \quad (14)$$

Proof. Using definition of v_t , we have

$$\begin{aligned}
\mathbb{E} \left[\|v_t\|_{\hat{D}_t^{-1}}^2 \right] &= \mathbb{E} \left[\|\nabla f_{i_t}(w_t) - \nabla f_{i_t}(z_t) + \nabla P(z_t)\|_{\hat{D}_t^{-1}}^2 \right] \\
&\leq 3\mathbb{E} \left[\|\nabla P(w_t)\|_{\hat{D}_t^{-1}}^2 \right] + 3\mathbb{E} \left[\|\nabla P(w_t) - \nabla P(z_t)\|_{\hat{D}_t^{-1}}^2 \right] \\
&\quad + 3\mathbb{E} \left[\|\nabla f_{i_t}(w_t) - \nabla f_{i_t}(z_t)\|_{\hat{D}_t^{-1}}^2 \right] \\
&\leq 3\mathbb{E} \left[\|\nabla P(w_t)\|_{\hat{D}_t^{-1}}^2 \right] + \frac{6L^2}{\alpha} \mathbb{E} \left[\|w_t - z_t\|^2 \right].
\end{aligned}$$

Here we use Assumption 1 and $\hat{D}_t^{-1} \preceq \frac{1}{\alpha} I$. □

Theorem 7 (Theorem 1). Suppose that Assumption 1 holds, let $\varepsilon > 0$, let p denote the probability and let the step-size satisfy

$$\eta \leq \min \left\{ \frac{\alpha}{4L}, \frac{\sqrt{p}\alpha}{\sqrt{24L}}, \frac{p^{2/3}}{144^{2/3}} \frac{\alpha}{L} \right\}.$$

Given an initial point $w_0 \in \mathbb{R}^d$, let $\Delta_0 = P(w_0) - P^*$. Then the number of iterations performed by Scaled L-SVRG, starting from w_0 , required to obtain an ε -approximate solution of non-convex finite-sum problem (1) can be bounded by

$$T = \mathcal{O} \left(\frac{\Gamma}{\alpha} \frac{L\Delta_0}{p^{2/3}\varepsilon^2} \right).$$

Proof. Using L -smoothness of the function P and $I \preceq \frac{1}{\alpha} \hat{D}_t$, we have

$$\begin{aligned}
\mathbb{E} [P(w_{t+1})] &\leq \mathbb{E} [P(w_t)] + \mathbb{E} [\langle \nabla P(w_t), w_{t+1} - w_t \rangle] + \frac{L}{2} \mathbb{E} [\|w_{t+1} - w_t\|^2] \\
&\leq \mathbb{E} [P(w_t)] + \mathbb{E} [\langle \nabla P(w_t), w_{t+1} - w_t \rangle] + \frac{L}{2\alpha} \mathbb{E} [\|w_{t+1} - w_t\|_{\hat{D}_t}^2].
\end{aligned}$$

Taking into account an update of Scaled L-SVRG, we obtain

$$\begin{aligned}
\mathbb{E} [P(w_{t+1}) - P^*] &\leq \mathbb{E} [P(w_t) - P^*] + \mathbb{E} [\langle \nabla P(w_t), -\eta \hat{D}_t^{-1} v_t \rangle] + \frac{L\eta^2}{2\alpha} \mathbb{E} [\|v_t\|_{\hat{D}_t^{-1}}^2] \\
&= \mathbb{E} [P(w_t) - P^*] - \eta \mathbb{E} [\langle \nabla P(w_t), \hat{D}_t^{-1} \nabla P(w_t) \rangle] + \frac{L\eta^2}{2\alpha} \mathbb{E} [\|v_t\|_{\hat{D}_t^{-1}}^2].
\end{aligned}$$

Let us define $\Phi_{t+1} = P(w_{t+1}) - P^* + A\|w_{t+1} - z_{t+1}\|^2$ for some $A > 0$. Using Lemmas 6, 7, we

have

$$\begin{aligned}
\mathbb{E} [\Phi_{t+1}] &\leq \mathbb{E} [P(w_t) - P^*] - \eta \mathbb{E} \left[\|\nabla P(w_t)\|_{\hat{D}_t^{-1}}^2 \right] + \frac{L\eta^2}{2\alpha} \mathbb{E} \left[\|v_t\|_{\hat{D}_t^{-1}}^2 \right] \\
&\quad + A \mathbb{E} [\|w_{t+1} - z_{t+1}\|^2] \\
&\leq \mathbb{E} [P(w_t) - P^*] - \eta \mathbb{E} \left[\|\nabla P(w_t)\|_{\hat{D}_t^{-1}}^2 \right] + \eta^2 \left(\frac{L}{2\alpha} + \frac{A}{\alpha} \right) \mathbb{E} \left[\|v_t\|_{\hat{D}_t^{-1}}^2 \right] \\
&\quad + A(1-p)(1+\eta B) \mathbb{E} [\|w_t - z_t\|^2] + A(1-p) \frac{\eta}{\alpha B} \mathbb{E} \left[\|\nabla P(w_t)\|_{\hat{D}_t^{-1}}^2 \right] \\
&\leq \mathbb{E} [P(w_t) - P^*] - \eta \left(1 - \frac{A(1-p)}{\alpha B} \right) \mathbb{E} \left[\|\nabla P(w_t)\|_{\hat{D}_t^{-1}}^2 \right] \\
&\quad + A(1-p)(1+\eta B) \mathbb{E} [\|w_t - z_t\|^2] \\
&\quad + \eta^2 \left(\frac{L}{2\alpha} + \frac{A}{\alpha} \right) \left(2 \mathbb{E} \left[\|\nabla P(w_t)\|_{\hat{D}_t^{-1}}^2 \right] + \frac{2L^2}{\alpha} \mathbb{E} [\|w_t - z_t\|^2] \right) \\
&\leq \mathbb{E} [P(w_t) - P^*] - \eta \left(1 - \frac{A(1-p)}{\alpha B} - \frac{2A}{\alpha} \eta - \frac{L}{\alpha} \eta \right) \mathbb{E} \left[\|\nabla P(w_t)\|_{\hat{D}_t^{-1}}^2 \right] \\
&\quad + A \left((1-p)(1+\eta B) + \eta^2 \left(\frac{L}{A} + 2 \right) \frac{L^2}{\alpha^2} \right) \mathbb{E} [\|w_t - z_t\|^2]. \tag{15}
\end{aligned}$$

We need to choose A , η , B in such way:

$$1 - \frac{A(1-p)}{\alpha B} - \frac{2A}{\alpha} \eta - \frac{L}{\alpha} \eta \geq \frac{1}{4}; \quad (1-p)(1+\eta B) + \eta^2 \left(\frac{L}{A} + 2 \right) \frac{L^2}{\alpha^2} \leq 1.$$

Thus, taking

$$A = \frac{3\eta^2 L^3}{p\alpha^2}; \quad B = \frac{p}{3\eta}; \quad \eta \leq \min \left\{ \frac{1}{4}, \left(\frac{p}{6} \right)^{1/2}, \left(\frac{p}{6} \right)^{2/3} \right\} \frac{\alpha}{L},$$

we have

$$\mathbb{E} [\Phi_{t+1}] \leq \mathbb{E} [\Phi_t] - \frac{\eta}{4} \mathbb{E} \left[\|\nabla P(w_t)\|_{\hat{D}_t^{-1}}^2 \right].$$

Summing up and using that \hat{w}_T is chosen uniformly from all w_t from 0 to $T-1$, we get

$$\mathbb{E} \|\nabla P(\hat{w}_T)\|^2 \leq \Gamma \mathbb{E} \|\nabla P(\hat{w}_T)\|_{\hat{D}_T^{-1}}^2 \leq \frac{4\Delta_0 \Gamma}{T\eta} \leq \max \left\{ 1, \sqrt{\frac{6}{p}}, \frac{\sqrt[3]{36}}{p^{2/3}} \right\} \frac{4L\Delta_0 \Gamma}{T} \frac{\Gamma}{\alpha}.$$

Then

$$T = \mathcal{O} \left(\frac{\Gamma L \Delta_0}{\alpha p^{2/3} \varepsilon^2} \right).$$

□

Theorem 8 (Theorem 4). Suppose that Assumptions 1 and 2 hold, let $\varepsilon > 0$, let p denote the probability and let the step-size satisfy

$$\eta \leq \min \left\{ \frac{p\Gamma}{6\mu}, \frac{1}{4} \frac{\alpha}{L}, \left(\frac{p}{6} \right)^{1/2} \frac{\alpha}{L}, \left(\frac{p}{6} \right)^{2/3} \frac{\alpha}{L} \right\}.$$

Then the number of iterations performed by Scaled L-SVRG sufficient for finding an ε -

approximate solution of non-convex finite-sum problem (1) can be bounded by

$$T = \mathcal{O} \left(\max \left\{ \frac{1}{p}, \frac{\Gamma}{\alpha} \frac{L}{p^{2/3}\mu} \right\} \right).$$

Proof. Starting from (15), we get

$$\begin{aligned} \mathbb{E} [\Phi_{t+1}] &\leq \mathbb{E} [P(w_t) - P^*] - \eta \left(1 - \frac{A(1-p)}{\alpha B} - \frac{2A}{\alpha} \eta - \frac{L}{\alpha} \eta \right) \mathbb{E} \left[\|\nabla P(w_t)\|_{\hat{D}_t^{-1}}^2 \right] \\ &\quad + A \left((1-p)(1+\eta B) + \eta^2 \left(\frac{L}{A} + 2 \right) \frac{L^2}{\alpha^2} \right) \mathbb{E} [\|w_t - z_t\|^2]. \end{aligned}$$

We use $\frac{1}{\Gamma} I \preceq \hat{D}_t^{-1}$ and Assumption 2 and then get

$$\begin{aligned} \mathbb{E} [\Phi_{t+1}] &\leq \mathbb{E} [P(w_t) - P^*] - \frac{\eta}{\Gamma} \left(1 - \frac{A(1-p)}{\alpha B} - \frac{2A}{\alpha} \eta - \frac{L}{\alpha} \eta \right) \mathbb{E} [\|\nabla P(w_t)\|^2] \\ &\quad + A \left((1-p)(1+\eta B) + \eta^2 \left(\frac{L}{A} + 2 \right) \frac{L^2}{\alpha^2} \right) \mathbb{E} [\|w_t - z_t\|^2] \\ &\leq \mathbb{E} [P(w_t) - P^*] - \frac{\eta\mu}{\Gamma} \left(1 - \frac{A(1-p)}{\alpha B} - \frac{2A}{\alpha} \eta - \frac{L}{\alpha} \eta \right) \mathbb{E} [P(w_t) - P^*] \\ &\quad + A \left((1-p)(1+\eta B) + \eta^2 \left(\frac{L}{A} + 2 \right) \frac{L^2}{\alpha^2} \right) \mathbb{E} [\|w_t - z_t\|^2]. \end{aligned}$$

We need to choose A , η , B in such way:

$$1 - \frac{A(1-p)}{\alpha\beta} - \frac{2A}{\alpha} \eta - \frac{L}{\alpha} \eta \geq \frac{1}{4}; \quad (1-p)(1+\eta\beta) + \eta^2 \left(\frac{L}{A} + 2 \right) \frac{L^2}{\alpha^2} \leq 1 - \frac{\mu\eta}{4\Gamma}.$$

Thus, taking

$$A = \frac{3\eta^2 L^3}{p\alpha^2}; \quad \beta = \frac{p}{3\eta}; \quad \eta \leq \min \left\{ \frac{p\Gamma}{6\mu}, \frac{1}{4} \frac{\alpha}{L}, \left(\frac{p}{6} \right)^{1/2} \frac{\alpha}{L}, \left(\frac{p}{6} \right)^{2/3} \frac{\alpha}{L} \right\},$$

we have

$$\mathbb{E} [\Phi_{t+1}] \leq \left(1 - \min \left\{ \frac{p}{24}, \frac{1}{16} \frac{\alpha\mu}{\Gamma L}, \left(\frac{p}{6} \right)^{1/2} \frac{\alpha\mu}{4\Gamma L}, \left(\frac{p}{6} \right)^{2/3} \frac{\alpha\mu}{4\Gamma L} \right\} \right) \mathbb{E} [\Phi_t].$$

Running the recursion, using the notation of $\Phi_t = P(w_t) - P^* + A\|w_t - z_t\|^2$ and $w_0 = z_0$, we obtain

$$\begin{aligned} \mathbb{E} [P(w_T) - P^*] &\leq \mathbb{E} [\Phi_T] \\ &\leq \left(1 - \min \left\{ \frac{p}{24}, \frac{1}{16} \frac{\alpha\mu}{\Gamma L}, \left(\frac{p}{6} \right)^{1/2} \frac{\alpha\mu}{4\Gamma L}, \left(\frac{p}{6} \right)^{2/3} \frac{\alpha\mu}{4\Gamma L} \right\} \right)^T \Phi_0 \\ &= \left(1 - \min \left\{ \frac{p}{24}, \frac{1}{16} \frac{\alpha\mu}{\Gamma L}, \left(\frac{p}{6} \right)^{1/2} \frac{\alpha\mu}{4\Gamma L}, \left(\frac{p}{6} \right)^{2/3} \frac{\alpha\mu}{4\Gamma L} \right\} \right)^T \Delta_0. \end{aligned}$$

Then, to achieve $\mathbb{E}[P(w_T) - P^*] \leq \varepsilon$, we need

$$T = \mathcal{O} \left(\max \left\{ \frac{1}{p}, \frac{\Gamma}{\alpha} \frac{L}{p^{2/3}\mu} \right\} \log \frac{\Delta_0}{\varepsilon} \right) \text{ iterations.}$$

□

F The role of β in the preconditioner

The purpose of this section is to better understand the role that β plays with regards to the convergence theory and practical performance of our algorithms. Recall that β is the momentum parameter for the preconditioner (4), and it controls the weighting/trade-off between the past curvature history and the current minibatch Hessian.

Note that the analysis presented in Appendices D and E does not impose any additional assumptions on β , which demonstrates a kind of universality of our method and convergence theory. Note that, Adam [Défossez et al., 2020] and OASIS do not have such universality. In particular, for Adam, the parameter β_2 (corresponding to β in this work) is critical: for Adam to converge at the rate $1/\sqrt{T}$ in the non-convex setting, one must choose $\beta_2 = 1 - 1/\sqrt{T}$, while for small β_2 the method diverges [Reddi et al., 2019]. The dependence of OASIS on β is only presented in the adaptive case, but this dependence can negatively impact, or destroy, convergence. This section aims to better understand the choice β .

Consider the following quadratic function:

$$f(x, y) = L \left(\frac{x+y}{2} \right)^2 + \mu \left(\frac{x-y}{2} \right)^2. \quad (16)$$

The corresponding Hessian for this function is

$$\nabla^2 f(x, y) = \begin{pmatrix} \frac{L+\mu}{2} & \frac{L-\mu}{2} \\ \frac{L-\mu}{2} & \frac{L+\mu}{2} \end{pmatrix},$$

and

$$\text{diag}(z_t \odot \nabla^2 f z_t) = \begin{pmatrix} \frac{L+\mu}{2} + \frac{L-\mu}{2} z_t^1 z_t^2 & 0 \\ 0 & \frac{L+\mu}{2} + \frac{L-\mu}{2} z_t^1 z_t^2 \end{pmatrix},$$

where z_t is from a Radermacher distribution. One can note that with probability $\frac{1}{2}$ our approximation $\text{diag}(z_t \odot \nabla^2 f z_t)$ is

$$\begin{pmatrix} L & 0 \\ 0 & L \end{pmatrix} \quad \text{or} \quad \begin{pmatrix} \mu & 0 \\ 0 & \mu \end{pmatrix}. \quad (17)$$

F.1 The worst case

Intuitively, with a good understanding of β , it should be possible to get better practical performance of the method. For example, our convergence analysis depends upon the factor Γ/α (recall Remark 1), and a good choice of β can shrink this factor. However, here we present the worst case, and show that for the function described above, unfortunately, improvement is not possible. Choose $\alpha > \mu$, so that for \hat{D}_t we have two possible matrices with probability $\frac{1}{2}$:

$$\begin{pmatrix} L & 0 \\ 0 & L \end{pmatrix} \quad \text{or} \quad \begin{pmatrix} \alpha & 0 \\ 0 & \alpha \end{pmatrix}.$$

The matrices above are scaled identity matrices, it means that applying the preconditioner is equivalent to simply dividing the gradient in the well-known GD by a constant. Note that the original problem (16) is L -smooth, then the choice of the stepsize of the method proportional to $\eta = 1/L$ seems classical and justified. But the scaling can dramatically change size of gradient especially when $\beta = 0$. In particular, when we work with the second matrix we change gradient by $1/\alpha$. Then if we take the previous step $\eta = 1/L$, we can significantly escape from the solution for rather small $\alpha < 1/2$, since in this case the effective stepsize is no longer $1/L$, but $1/(\alpha L) > 2/L$. Then it is really worth taking a step $\eta \sim \frac{\alpha}{L}$. Importantly, using $\beta \approx 1$ can fix the raised issue, but we did not impose additional conditions on β in the analysis of Algorithms 1 and 2. Therefore, in the case of arbitrary β (in particular, $\beta = 0$), our analysis of Algorithms 1 and 2 looks like unimprovable. But an interesting direction for future research is more careful theoretical tuning of β .

F.2 How to choose the constant β

D_t is a linear combination of identically distributed independent matrices (17). In such a situation, it is natural to consider reducing the variance of D_t . Note that

$$D_t = \beta^t \mathbf{diag}(z_0 \odot \nabla^2 f z_0) + \sum_{\tau=1}^t \beta^{t-\tau} (1-\beta) \mathbf{diag}(z_\tau \odot \nabla^2 f z_\tau).$$

and notice that, by (17), every $\mathbf{diag}(z_\tau \odot \nabla^2 f z_\tau)$ has the same distribution. Then the variance of D_t can be computed as

$$\text{Var}[D_t] = \left[\beta^{2t} + \sum_{\tau=1}^t \beta^{2t-2\tau} (1-\beta)^2 \right] C,$$

where C is some constant (that does not depend on β). Now, minimizing this expression w.r.t. $\beta \in [0; 1]$:

$$\min_{\beta \in [0; 1]} \left[\beta^{2t} + \sum_{\tau=1}^t \beta^{2t-2\tau} (1-\beta)^2 \right].$$

Using the optimality conditions one has:

$$\beta^{2t-1} (2t - 1 + 2t\beta + 2) = 1.$$

If we have a limit of iterations T and if we want to minimize the variance of the final preconditioner, we can take

$$\beta = \frac{1}{2^T \sqrt[2T]{2T - 1 + 2T\beta + 2}} \sim \frac{1}{2^T \sqrt[2T]{2T}} \xrightarrow{T \rightarrow \infty} 1.$$

F.3 It is better to consider varying β_t

As in the previous section, here we also want to reduce the variance of D_t . But now, let us consider the case when β_t is allowed to vary:

$$D_t = \beta_t D_{t-1} + (1 - \beta_t) \mathbf{diag}(z_t \odot \nabla^2 f z_t).$$

To understand how to choose β_t , note that at each iteration, because $\mathbf{diag}(z_t \odot \nabla^2 f z_t)$ we get one of the two matrices given in (17). To reduce the variance of the matrix D_t one can choose D_t as

$$D_t = \frac{1}{t+1} \sum_{\tau=0}^t \mathbf{diag}(z_\tau \odot \nabla^2 f z_\tau) = \frac{t}{t+1} D_{t-1} + \frac{1}{t+1} \mathbf{diag}(z_t \odot \nabla^2 f z_t).$$

Thus,

$$\beta_t = 1 - \frac{1}{t+1}.$$

Using the identity and independence of the $\text{diag}(z_\tau \odot \nabla^2 f z_\tau)$ distributions, one can note that such a β_t gives better variance than the constant β from the previous subsection.